Global *k*-space analysis of electron-phonon interaction in graphene and application to *M*-point spectroscopy

Rolf Binder,[1,2] Adam T. Roberts,[1,3] Nai H. Kwong,[1] Arvinder Sandhu,[1,2] and Henry O. Everitt[3,4]
[1]*College of Optical Sciences, University of Arizona, Tucson, Arizona 85721, USA*
[2]*Department of Physics, University of Arizona, Tucson, Arizona 85721, USA*
[3]*U.S. Army Aviation and Missile Research, Development, and Engineering Center, Redstone Arsenal, Alabama 35898, USA*
[4]*Department of Physics, Duke University, Durham, North Carolina 27708, USA*
(Received 23 October 2015; published 8 February 2016)

Recently, optical probes have become available that can access and observe energy renormalization due to electron-phonon interaction in graphene away from the well-studied Dirac *K* point. Using an expanded deformation potential approach, we present a theoretical study of the electron-phonon self-energy and scattering matrix elements across the entire Brillouin zone. We elucidate the roles of modulated hopping and conventional deformation potential coupling, parameterized via standard deformation potentials, the in-plane phonon modes, intra- and interband contributions, and umklapp processes. Applying the theory to nonlinear optical transmission spectroscopy in the vicinity of the *M* point, we find very good agreement with recently published experimental data.

DOI: 10.1103/PhysRevB.93.085414

I. INTRODUCTION

Graphene is widely recognized as a transformative material system for the development of new electronic and photonic devices including high-speed field-effect transistors, efficient terahertz sources, ultrafast broadband photodetectors, modulators, plasmonic devices, and photodetectors (for example, Refs. [1–15]). The fundamental electronic, vibronic, and optical properties are, by now, well understood (e.g., Refs. [16–18]). In particular, much effort has been spent on Raman spectroscopy [19–23], linear and nonlinear spectroscopy close to the Dirac point including THz spectroscopy and generation (e.g., Refs. [24–42]), electron-electron interactions (e.g., Refs. [43,44]), phonons (e.g., Refs. [45–49]), electron-phonon interactions (e.g., Refs. [50–56]), and linear and nonlinear spectroscopy close to the saddle point (e.g., Refs. [40,57–61]). Recently, increasing emphasis has been put on the understanding of differential optical transmission spectra that are negative; in other words, on the increase of absorption caused by optical pumping [35–37,61,62]. Negative differential transmission is usually related to complex many-body effects, in contrast to optically induced phase-space filling that leads to positive differential transmission. We will comment on this effect below in the context of spectroscopy close to the saddle point (*M* point), Sec. V.

As mentioned, the theory of phonon spectra and electron-phonon interactions in graphene has been well studied. The theoretical work can be broadly grouped into two classes, first-principles theories (density-functional theory, DFT) on the one hand, and explicit models for the dynamical matrices and effective electron-phonon Hamiltonians on the other. Both approaches have their advantages. The DFT models are nominally without fitting parameters, although in practice specific implementations and even the number of points used in numerical integrations can influence the results. However, the disadvantage is a potential lack of transparency because publications usually do not include the exact theoretical formulas. Explicit models always have fitting parameters, making them less predictive, at least regarding their quantitative predictions; qualitative predictions are frequently independent of the fitting parameters' values. However, conceptual and mathematical simplicity and transparency is an advantage of those approaches. For example, the authors of Ref. [63] point out that their dynamical matrix for the graphene phonon spectrum is not meant to improve on the phonon spectra obtained in Ref. [45], but to give a "simpler alternative for the phonon spectrum." A similar dynamical matrix was also used in Ref. [64]. Other studies of electron-phonon coupling involving explicit phonon models include [65,66], where the role of zone-boundary phonons has been elucidated. Explicit models for the electron-phonon coupling, formulated in terms of the electron self-energy, include [51,67–69], a related Boltzmann transport theory approach and mobility analysis was used in Refs. [70–74], the role of out-of-plane phonons was studied in Ref. [75], and the self-energy for optical phonons was investigated in Ref. [76]. First-principles studies of phonon spectra include [77], phonon anharmonicities were studied in Ref. [78], and first-principles studies of phonons and electron-phonon coupling include [52,53,79–82].

Among the explicit theories for electron-phonon interactions are the so-called deformation potential models that are important because of their simplicity. They allow easy comparison across disciplines like electrical and thermal transport as well as optics, while being able to capture at least some general and possibly robust features of electron-phonon scattering. Within the class of deformation potential models, we need to distinguish between the conventional deformation potential theory, which can be found in many solid-state textbooks (e.g., Ref. [83]), and those that, in the context of graphene, may be called modulated hopping (or gauge field coupling), developed in Refs. [84–87]. In the following, we will reserve the term deformation potential (DP) theory to the conventional, textbook deformation potential theories, and for the other use the term modulated hopping (MH). Common to the deformation potential theories is that they typically involve a small number of parameters.

As optical probes capable of accessing almost arbitrary points in the Brillouin zone (BZ) become more widely

available, it becomes increasingly important to establish a good understanding of electron-phonon interaction, especially deformation potential models that are not limited to the vicinity of the Dirac point. In this paper, we present a detailed study of an expanded deformation potential model that includes both modulated hopping (MH) and conventional deformation potential (DP) coupling. We pay particular attention to the electron-phonon processes that involve BZs other than the first zone. The expanded model, which is based on a commonly used Hamiltonian for on-site and nearest-neighbor coupling, leads to a DP/MH model that generalizes well-established forms valid near the Dirac point. We discuss this limiting process not only for the purposes of identifying our parameters with those already existing in the literature, but also to use literature results based on first-principles theories to obtain reasonable parameter values. As shown below, in contrast to MH, which includes only one parameter, the case of DP is more complex, as that coupling requires a physically motivated cutoff in reciprocal space in order to be well defined. We discuss the physical motivation for this and derive a reasonable functional form for the wave-vector-dependent DP model.

Our numerical results include phonon frequencies and eigenvectors calculated over the entire BZ from the diagonalization of a dynamic matrix [64]. We present calculated self-energies, relevant for transport and optical properties, as well as differential self-energies relevant for nonlinear differential spectroscopy across the entire BZ. We also present scattering matrix elements for the various phonon modes. The matrix elements for LA and LO exhibit discontinuities in the electronic BZ, which can be understood as a result of phonon dispersion degeneracies on the boundary of the phonon BZ. As a specific application, we calculate differential transmission spectra for nonlinear M-point spectroscopy and compare the results to recently published experimental data. We find that these results are in even better agreement than previous results that were based on the concept of effective deformation potentials. We also discuss this concept and its relation to the much more general theory employed in this paper, which involves both kinds of coupling processes (i.e., MH and DP), and all in-plane phonon modes (i.e., TA, LA, LO, TO).

This paper is organized as follows. We begin by introducing the necessary definitions and conventions by which our expanded deformation potential model is constructed (Sec. II A). We then derive the Hamiltonians and self-energies for the deformation potential and modulated hopping components of this larger model and compare its predictions against salient approaches in the literature that primarily address the Dirac K point (Secs. II B and III). Having established this consistency, we then explore the predictions of this expanded deformation potential model at other regions of the BZ, most notably at the M point. We focus on transition matrix elements and electronic self-energies in Sec. IV, and on recently published ultraviolet pump-probe differential transmission spectroscopic measurements in Sec. V. We conclude with three appendices that provide additional information about the microscopic motivation of our model, the phonon model used throughout the manuscript, and the contribution of higher BZs and avoidance of unphysical divergences.

II. EXPANDED DEFORMATION POTENTIAL MODEL

A. Definitions

Let us start with a Hamiltonian in the basis of localized electrons that can be regarded as a purely phenomenological description of the system. All parameters will be fixed either through comparisons with experiments or with completely predictive theories. In Appendix A, we will discuss options to fix some of the free parameters by viewing how the general Hamiltonian is derived from a more basic physical starting point. Our phenomenological Hamiltonian, restricted to on-site energies and nearest-neighbor hopping terms, reads as

$$H = \sum_{jn\sigma} \varepsilon_{2p} c^{\dagger}_{jn\sigma} c_{jn\sigma} - \sum_{\langle jn, j'n'\rangle\sigma} t c^{\dagger}_{jn\sigma} c_{j'n'\sigma}, \tag{1}$$

where ε_{2p} is the on-site energy of the $2p$ electrons in the graphene lattice (not the $2p$ energy of the individual carbon atoms), t is the hopping (or transfer) integral, and $\langle jn, j'n'\rangle$ denotes summation over nearest neighbor pairs. The creation (annihilation) operators $c^{\dagger}_{jn\sigma}$ ($c_{jn\sigma}$) are labeled by the unit cell index j, the basis atom index $n = 1,2$, and the spin σ. The on-site energy ε_{2p} of an electron at site j,n can be thought of as having a kinetic energy contribution at site j,n as well as an electron-ion interaction contribution of the form

$$\begin{aligned} W_{\text{el-ion}}(\mathbf{r})|_{\mathbf{r}=\mathbf{R}_{jn}} &= -\sum_{j'n'} W(\mathbf{r} - \mathbf{R}_{j'n'})|_{\mathbf{r}=\mathbf{R}_{jn}} \\ &= -\sum_{j'n'} W(\mathbf{R}_{jn} - \mathbf{R}_{j'n'}), \end{aligned} \tag{2}$$

where $\mathbf{R}_{jn}$ is the position vector of the ion at the site n,j. The condition $\mathbf{r} = \mathbf{R}_{jn}$ means the electron orbital at site n,j moves rigidly with the ion at that site. The hopping parameter t is assumed to be a function of the nearest-neighbor distance, i.e., $t = t(|\mathbf{R}_{jn} - \mathbf{R}_{j'n'}|)$, where it is implied that the site indices are restricted to nearest neighbor pairs. We denote the ion positions as $\mathbf{R}_{jn} = \mathbf{R}^{(0)}_{jn} + \vec{\xi}_{jn}$, where $\mathbf{R}^{(0)}_{jn}$ are the two-dimensional equilibrium lattice position vectors ($\mathbf{R}^{(0)}_{j1} = \mathbf{R}^{(0)}_{j}$, $\mathbf{R}^{(0)}_{j2} = \mathbf{R}^{(0)}_{j} + \vec{\delta}_1$, $\mathbf{R}^{(0)}_{j} = j_1\mathbf{a}_1 + j_2\mathbf{a}_2$), and $\vec{\xi}_{jn}$ are the displacements due to lattice vibrations. Our notational convention for defining various lattice vectors in real and reciprocal spaces is shown in Fig. 1. We follow Ref. [17] and use a coordinate convention in which the hexagons in real space have horizontal lines and those in reciprocal space have vertical lines. Specifically, the nearest-neighbor vectors are

$$\vec{\delta}_1 = \frac{a}{2}(1,\sqrt{3}), \quad \vec{\delta}_2 = \frac{a}{2}(1,-\sqrt{3}), \quad \vec{\delta}_3 = a(-1,0).$$

The primitive translation vectors in real space are

$$\mathbf{a}_1 = \frac{a}{2}(3,\sqrt{3}), \quad \mathbf{a}_2 = \frac{a}{2}(3,-\sqrt{3}),$$

and in reciprocal space are

$$\mathbf{b}_1 = \frac{2\pi}{3a}(1,\sqrt{3}), \quad \mathbf{b}_2 = \frac{2\pi}{3a}(1,-\sqrt{3}),$$

where a is the carbon-carbon bondlength ($a = 1.42$ Å), which is related to the lattice constant a_L via $a_L = \sqrt{3}a$.

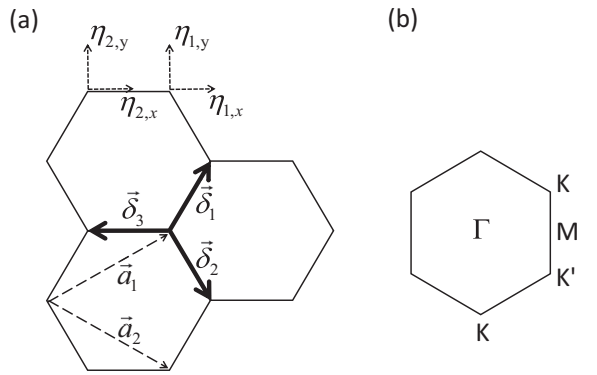

FIG. 1. Definition of (a) primitive translation vectors $\vec{a}$, nearest-neighbor vectors $\vec{\delta}$, phonon mode vectors $\vec{\eta}$ defined through Eq. (12), and (b) Brillouin zone used in this paper.

We obtain the electron phonon interaction (e.g., Refs. [83,84]) by writing the on-site energy in Eq. (1) as

$$\varepsilon_{2p} \to \varepsilon^0_{2p} - \sum_{j'n'} \left[W(\mathbf{R}_{jn} - \mathbf{R}_{j'n'}) - W\left(\mathbf{R}^{(0)}_{jn} - \mathbf{R}^{(0)}_{j'n'}\right)\right], \quad (3)$$

where $\varepsilon^0_{2p} = \varepsilon_{2p}(\mathbf{R}_{jn} = \mathbf{R}^{(0)}_{jn})$, and the hopping energy as

$$t \to t_0 + (t - t_0), \quad (4)$$

where $t_0 = t(|\mathbf{R}^{(0)}_{jn} - \mathbf{R}^{(0)}_{j'n'}|)$ and $t = t(|\mathbf{R}_{jn} - \mathbf{R}_{j'n'}|)$. To the first order in the displacements, we have the Hamiltonian for the DP term,

$$H_{\rm DP} = -\frac{1}{A} \sum_{jn\sigma j'n'\mathbf{q}} i\mathbf{q} \cdot (\vec{\xi}_{jn} - \vec{\xi}_{j'n'}) \times e^{i\mathbf{q}\cdot(\mathbf{R}^{(0)}_{jn} - \mathbf{R}^{(0)}_{j'n'})} W(\mathbf{q}) c^\dagger_{jn\sigma} c_{jn\sigma} \quad (5)$$

after writing the potential energy W in terms of its two-dimensional Fourier transform, $W(\mathbf{r}) = (1/A)\sum_{\mathbf{q}} e^{i\mathbf{q}\cdot\mathbf{r}} W(\mathbf{q})$. Here, A is the area of the system, and the index DP stands for deformation potential, by which we mean the conventional deformation potential discussed in most solid state text books. We note that it is customary to take only the second term with $\vec{\xi}_{j'n'}$ in Eq. (5) for the deformation potential approximation called Nordheim's rigid ion model (e.g., Refs. [83,88,89]). The argument for this is that in the general electron-ion interaction, which is of the form $W_{\text{el-ion}}(\mathbf{r}) = -\sum_{j'n'} W(\mathbf{r} - \mathbf{R}_{j'n'})$, only the ion positions $\mathbf{R}_{j'n'}$ should be displaced, not the electron positions $\mathbf{r}$. One might wonder if this is always appropriate, especially in the case of strongly localized electron orbitals for which the Hamiltonian (1) is designed. In other words, if the electron always moves with the ion, there would be a contribution to the electron-phonon interaction that corresponds to the displacement of $\mathbf{r}$, which in turn is "slaved" to the displacement of the ion at $\mathbf{R}_{jn}$. Below, we will argue that this is not of practical importance in the present case because the contribution from $\vec{\xi}_{jn}$ in Eq. (5) turns out to be small compared to the $\vec{\xi}_{j'n'}$ contribution.

Furthermore, the first-order expansion in $\vec{\xi}_{jn}$ of the hopping term in the Hamiltonian yields

$$H_{\rm MH} = -\left.\frac{\partial t}{\partial r}\right|_0 \frac{1}{a} \sum_{\langle jn, j'n'\rangle\sigma} \left[\mathbf{R}^{(0)}_{jn} - \mathbf{R}^{(0)}_{j'n'}\right] \cdot [\vec{\xi}_{jn} - \vec{\xi}_{j'n'}] c^\dagger_{jn\sigma} c_{j'n'\sigma}, \quad (6)$$

where the subscript MH stands for modulated hopping, and the spatial gradient of the hopping parameter, $\vec{\nabla} t(r) = (\partial t/\partial r)\mathbf{r}/r$, $\frac{\partial t}{\partial r}|_0 = \frac{\partial t}{\partial r}|_{r=|\mathbf{R}^{(0)}_{jn} - \mathbf{R}^{(0)}_{j'n'}|}$, and $|\mathbf{R}^{(0)}_{jn} - \mathbf{R}^{(0)}_{j'n'}| = a$, has been used. We now define the deformation potentials as follows. For the conventional deformation potential, we use

$$D_{\rm DP} = \frac{2}{A_0} W(\mathbf{0}), \quad (7)$$

$$D_{\rm DP}(\mathbf{q}) = D_{\rm DP} \frac{W(\mathbf{q})}{W(\mathbf{0})} = \frac{2}{A_0} W(\mathbf{q}), \quad (8)$$

and for the modulated hopping, we use

$$D_{\rm MH} = \frac{3}{4} \left.\frac{\partial t}{\partial r}\right|_0 a. \quad (9)$$

An estimate for $D_{\rm MH}$ could be based on the bondlength derivative of the bond energy, which in Ref. [90] is found to be -6.4 eV/Å. Using $a = 1.42$ Å, we have $D_{\rm MH} \simeq -6.82$ eV, which is, apart from the sign, slightly larger than the value of 2.5 eV used in Ref. [53]. At the end of Sec. III we further explore possible numerical values for $D_{\rm MH}$.

In conventional deformation potential theories, only the long-wavelength limit is important; therefore the deformation potential is one number, usually taken as $D_{\rm DP}(\mathbf{0})$, which is assumed to exhibit no singularity at $\mathbf{q} = \mathbf{0}$ as in metals. Wave-vector-dependent deformation potentials have been used, for example, by Woods and Mahan [63], and the issue of possible divergences in the long-wavelength limit has to be discussed for specific models. We discuss this in more detail in Appendix A. Since we want to keep the theory at a rather general, semiphenomenological level, we assume for the time being that the $\mathbf{q} \to \mathbf{0}$ limit exists. Furthermore, we will see shortly that the short-wavelength limit $|\mathbf{q}| \to \infty$ requires $D_{\rm DP}(\mathbf{q}) \to \mathbf{0}$. Quite generally, the interaction must be smooth on a subatomic length scale, leading to small or vanishing Fourier coefficients with wave vectors outside the first Brillouin zone). From a pragmatic point of view, the deformation potential may be characterized by two values rather than one: the value at $\mathbf{q} = 0$, and the approximate range in wave-vector space over which $W(\mathbf{q})$ is essentially nonzero. Alternatively, one can try to find specific models predicting the full $\mathbf{q}$ dependence, which is done in Appendix A. In terms of $D_{\rm DP}$ and $D_{\rm MH}$, the electron-phonon interactions are

$$H_{\rm DP} = -i\frac{1}{N} \sum_{jn\sigma j'n'\mathbf{q}} D_{\rm DP}(\mathbf{q})\mathbf{q} \cdot (\vec{\xi}_{jn} - \vec{\xi}_{j'n'}) e^{i\mathbf{q}\cdot(\mathbf{R}^{(0)}_{jn} - \mathbf{R}^{(0)}_{j'n'})} c^\dagger_{jn\sigma} c_{jn\sigma} \quad (10)$$

and

$$H_{\rm MH} = -\frac{4}{3a^2} D_{\rm MH} \sum_{\langle jn, j'n'\rangle\sigma} \left[\mathbf{R}^{(0)}_{jn} - \mathbf{R}^{(0)}_{j'n'}\right] \cdot [\vec{\xi}_{jn} - \vec{\xi}_{j'n'}] c^\dagger_{jn\sigma} c_{j'n'\sigma}, \quad (11)$$

where N is the number of carbon atoms, with $N/2 = A/A_0$ being the number of unit cells. Note that the $\mathbf{q}$ sum in Eq. (10) is not restricted to a Brillouin zone.

We next convert $H_{\rm DP}$ and $H_{\rm MH}$ in Eqs. (10) and (11) into a sum over the free phonon and Bloch electron eigenmodes. For this, the ionic displacements $\vec{\xi}_{jn}$ and electron operators $c_{jn\sigma}$

$(c^\dagger_{jn\sigma})$ are expanded in their respective eigenmodes. For $\vec{\xi}_{jn}$, standard phonon quantization theory [91] gives

$$\vec{\xi}_{jn} = \frac{i}{\sqrt{A}} \sum_{\mu,\mathbf{Q}\in BZ} e^{i\mathbf{Q}\cdot\mathbf{R}^{(0)}_{jn}} \vec{\eta}_{\mu n}(\mathbf{Q}) \sqrt{\frac{\hbar A_0}{2\omega^\mu_{\mathbf{Q}} M_c}} (d^\dagger_{-\mathbf{Q}\mu} + d_{\mathbf{Q}\mu}), \tag{12}$$

where $\omega^\mu_{\mathbf{Q}}$ are the phonon mode frequencies of branch μ at wave vector $\mathbf{Q}$, M_c is the mass of the ion, $d_{\mathbf{Q}\mu}$ ($d^\dagger_{\mathbf{Q}\mu}$) are the phonon annihilation (creation) operators, and $\vec{\eta}_{\mu n}(\mathbf{Q})$ are the two-dimensional phonon mode vectors. Below, we restrict ourselves to the in-plane transverse and longitudinal acoustic and optic modes, μ = TA,LA,LO,TO. A specific model for the phonon frequencies and mode vectors is given in Appendix B. The mode vectors are normalized,

$$\sum_{n=1}^{2} |\vec{\eta}_{\mu n}(\mathbf{Q})|^2 = 1,$$

and have the following symmetries within our convention for $\vec{\xi}_{jn}$ containing a factor of i. From the fact that the operators $\vec{\xi}_{jn}$ are Hermitian, it follows that

$$\vec{\eta}_{\mu n}(\mathbf{Q}) = -\vec{\eta}^*_{\mu n}(-\mathbf{Q}).$$

Moreover, given the lattice periodicity of the (classical) phonon Hamiltonian, $\vec{\eta}_{\mu n}(\mathbf{Q})$ satisfy the following relations under translations in reciprocal space (see Appendix B):

$$\vec{\eta}_{\mu 1}(\mathbf{Q}+\mathbf{G}) = \vec{\eta}_{\mu 1}(\mathbf{Q}), \tag{13}$$

$$e^{i\mathbf{G}\cdot\vec{\delta}_1} \vec{\eta}_{\mu 2}(\mathbf{Q}+\mathbf{G}) = \vec{\eta}_{\mu 2}(\mathbf{Q}), \tag{14}$$

where $\mathbf{G}$ is a reciprocal lattice vector. In practice, it is convenient to make one component, e.g., the y component of $\vec{\eta}_{\mu 1}(\mathbf{Q})$, purely real for all $\mathbf{Q}$.

Similarly, the localized electron operators are transformed to Bloch states,

$$c_{jn\sigma} = \sqrt{\frac{2}{N}} \sum_{\mathbf{k}\in BZ, s=\pm 1} e^{i\mathbf{k}\cdot(\mathbf{R}^{(0)}_j + \vec{\delta}_1 \delta_{n,2})} u_{\mathbf{k}sn} c_{\mathbf{k}s\sigma},$$

where $c_{\mathbf{k}s\sigma}$ denotes the electron annihilation operator for a Bloch electron in band s with two-dimensional crystal momentum $\hbar\mathbf{k}$, $\delta_{n,2}$ is the Kronecker delta, and $u_{\mathbf{k}sn}$ is the lattice-periodic part of the Bloch wave function. We are using here a well-established tight-binding approach, see for example [17,65,92]. Within this approach, we have two electronic bands, often called the π or valence band and π^* or conduction band. In our formalism, we denote the valence (conduction) band by $s = -1$ ($s = 1$). It is worth noting that the quality of this two-band approximation decreases with increasing photon energy, so care should be used in applying this formalism at the highest energies approaching the Γ point.

We work in the approximation of symmetric bands, related to the omission of next-nearest-neighbor hopping in Eq. (1). The band structure and Bloch coefficients in this approach are as follows. The band energy is given by $E^{(0)}_s(\mathbf{k}) = st|f'(\mathbf{k})|$, and the lattice-periodic part of the Bloch wave function is

$$\begin{pmatrix} u_{\mathbf{k}s1} \\ u_{\mathbf{k}s2} \end{pmatrix} = \frac{1}{\sqrt{2}} \begin{pmatrix} 1 \\ -se^{-i\phi(\mathbf{k})} \end{pmatrix}, \quad \begin{pmatrix} u_{\mathbf{k}+\mathbf{G}s1} \\ u_{\mathbf{k}+\mathbf{G}s2} \end{pmatrix} = \begin{pmatrix} u_{\mathbf{k}s1} \\ e^{-i\mathbf{G}\cdot\vec{\delta}_1} u_{\mathbf{k}s2} \end{pmatrix}, \tag{15}$$

where $\mathbf{k}$ is in the first Brillouin zone, and G is a reciprocal lattice vector. Here the function $f'(\mathbf{k})$ is given by

$$\begin{aligned} f'(\mathbf{k}) &= \sum_{i=1}^{3} e^{i\mathbf{k}\cdot\vec{\delta}_i} \\ &= 2\cos(k_x a/2)\cos(\sqrt{3}k_y a/2) + \cos(k_x a) \\ &\quad + i[2\sin(k_x a/2)\cos(\sqrt{3}k_y a/2) - \sin(k_x a)], \end{aligned} \tag{16}$$

and $\phi(\mathbf{k})$ is the phase of $f'(\mathbf{k})$. Explicitly, $f'(\mathbf{k}) = |f'(\mathbf{k})|e^{i\phi(\mathbf{k})}$ with

$$|f'(\mathbf{k})| = \sqrt{3 + 2\cos(\sqrt{3}k_y a) + 4\cos\left(\frac{3}{2}k_x a\right)\cos\left(\frac{\sqrt{3}}{2}k_y a\right)}, \tag{17}$$

$$\phi(\mathbf{k}) = \tan^{-1}\left[\frac{2\sin\left(\frac{k_x}{2}a\right)\cos\left(\frac{\sqrt{3}}{2}k_y a\right) - \sin(k_x a)}{2\cos\left(\frac{k_x}{2}a\right)\cos\left(\frac{\sqrt{3}}{2}k_y a\right) + \cos(k_x a)}\right]. \tag{18}$$

Before proceeding, we comment briefly on the sign of the hopping (or transfer) integral t. In Ref. [92] by Saito, Dresselhaus, and Dresselhaus (subscript SDD in the following), the 2×2 tight-binding Hamiltonian has off-diagonal elements $t_{\mathrm{SDD}} f'(\mathbf{k})$ [$f'(\mathbf{k})$ is called $f(\mathbf{k})$ there], and it is pointed out that t_{SDD} is negative. Our Hamiltonian (1) has a minus sign in front of t, so $t = -t_{\mathrm{SDD}}$. Hence t is positive. Since the magnitude of t can be assumed to decrease with increasing bond length (certainly $|t| \to 0$ as $a \to \infty$), we may assume that $\frac{\partial t}{\partial r}$ and hence D_{MH} are negative.

B. Hamiltonian and self-energy

In terms of the free phonon and Bloch electron modes, the deformation potential Hamiltonian Eq. (10) becomes

$$\begin{aligned} H_{\mathrm{DP}} = -\frac{1}{\sqrt{A}} \sum_{\substack{\mathbf{k}\mathbf{k}'\epsilon BZ \\ ss'\sigma\mu}} \left(\frac{\hbar A_0}{2M_c a^2 \omega^\mu_{\mathbf{k}-\mathbf{k}'}}\right)^{1/2} D_{\mathrm{DP}} W^{\mathrm{DP}}_\mu(\mathbf{k}s,\mathbf{k}'s') \\ \times [d^\dagger_{-\mathbf{k}+\mathbf{k}',\mu} + d_{\mathbf{k}-\mathbf{k}',\mu}] c^\dagger_{\mathbf{k}s\sigma} c_{\mathbf{k}'s'\sigma} \end{aligned} \tag{19}$$

with

$$\begin{aligned} W^{\mathrm{DP}}_\mu(\mathbf{k}s,\mathbf{k}'s') = \frac{1}{2}\sum_{\mathbf{G}\in\mathfrak{R}} \frac{W(\mathbf{k}-\mathbf{k}'-\mathbf{G})}{W(\mathbf{0})} a(\mathbf{k}-\mathbf{k}'-\mathbf{G}) \\ \cdot [\vec{\eta}_{\mu 1}(\mathbf{k}-\mathbf{k}') + \vec{\eta}_{\mu 2}(\mathbf{k}-\mathbf{k}')e^{i\mathbf{G}\cdot\vec{\delta}_1}] \\ \times \frac{1}{2}[1 + ss' e^{i(\phi(\mathbf{k})-\phi(\mathbf{k}')-\mathbf{G}\cdot\vec{\delta}_1)}], \end{aligned} \tag{20}$$

where $\mathfrak{R}$ denotes the set of reciprocal lattice vectors.

In calculating the $\mathbf{G}$ sum numerically, it is often more convenient to evaluate the phonon vectors only within one Brillouin zone and use Eqs. (13) and (14) to extrapolate to other zones. For each $\mathbf{Q}$, the diagonalization procedure determines

each eigenvector up to an overall phase, to which numerical routines may assign an arbitrary value, hence destroying the correct **G**-periodicity of the $\vec{\eta}_{\mu n}$. To facilitate computations following this method, we rewrite $W_\mu^{\rm DP}$ as

$$W_\mu^{\rm DP}(\mathbf{k}s,\mathbf{k}'s') = \frac{1}{2}\sum_{\mathbf{G}\in\mathfrak{R}} \frac{W(\mathbf{k}-\mathbf{k}'-\mathbf{G})}{W(\mathbf{0})} a(\mathbf{k}-\mathbf{k}'-\mathbf{G}) \cdot [\vec{\eta}_{\mu 1}(\mathbf{q}) + \vec{\eta}_{\mu 2}(\mathbf{q}) e^{-i(\mathbf{G}_u-\mathbf{G})\cdot\vec{\delta}_1}] \times \frac{1}{2}[1 + ss' e^{i(\phi(\mathbf{k})-\phi(\mathbf{k}')-\mathbf{G}\cdot\vec{\delta}_1)}], \tag{21}$$

where $\mathbf{q} = \mathbf{k} - \mathbf{k}' - \mathbf{G}_u$, and the reciprocal vector $\mathbf{G}_u$ is chosen such that $\mathbf{q}$ lies in the first Brillouin zone. A nonzero $\mathbf{G}_u$ signifies umklapp processes.

The last line in Eqs. (20) and (21) is a generalization of the well-known Bloch factor $\langle u_{\mathbf{k}s}|u_{\mathbf{k}'s'}\rangle = \frac{1}{2}(1 + ss' e^{i(\phi(\mathbf{k})-\phi(\mathbf{k}'))})$ to include contributions from phonons in Brillouin zones other than the first. These processes are determined by the range of $W(\mathbf{k}-\mathbf{k}'-\mathbf{G})$ in reciprocal space, which in principle could involve zones far away from the first BZ. They are more general than regular umklapp processes, in the sense that regular umklapp processes involve only zones adjacent to the first BZ.

In Eq. (19), we have used only the second term with $\vec{\xi}_{j'n'}$ in Eq. (5), which appears to be the standard approach (i.e., Nordheim's rigid ion model [83,88,89]). The first term with $\vec{\xi}_{jn}$ in Eq. (5) yields a correction of the form

$$H_{\rm DP,corr} = \frac{1}{\sqrt{A}} \sum_{\substack{\mathbf{k}\mathbf{k}'\epsilon BZ \\ ss'\sigma\mu}} \left(\frac{\hbar A_0}{2M_c a^2 \omega^\mu_{\mathbf{k}-\mathbf{k}'}}\right)^{1/2} \times \frac{1}{8}\sum_{\mathbf{G}\neq 0} D_{\rm DP}(\mathbf{G})[1 + e^{i\mathbf{G}\cdot\vec{\delta}_1}] a\mathbf{G}\cdot[\vec{\eta}_{\mu 1}(\mathbf{k}-\mathbf{k}') + ss'\vec{\eta}_{\mu 2}(\mathbf{k}-\mathbf{k}'-\mathbf{G}) e^{i(\phi(\mathbf{k})-\phi(\mathbf{k}'))}] \times [d^\dagger_{-\mathbf{k}+\mathbf{k}',\mu} + d_{\mathbf{k}-\mathbf{k}',\mu}] c^\dagger_{\mathbf{k}s\sigma} c_{\mathbf{k}'s'\sigma}. \tag{22}$$

This is a small correction because it excludes the first Brillouin zone from the integration over $D_{\rm DP}(\mathbf{k})$, and $D_{\rm DP}(\mathbf{k})$ is very small outside the first BZ. We show examples for $D_{\rm DP}(\mathbf{k})$ in Appendix A. In deriving Eqs. (19) and (22), we have used

$$\sum_{\mathbf{G}'} \Theta_{\rm BZ}(\mathbf{k}-\mathbf{k}'+\mathbf{G}+\mathbf{G}') = 1, \tag{23}$$

where $\Theta_{\rm BZ}(\mathbf{k}) = 1$ if $\mathbf{k}\in BZ$ and $\Theta_{\rm BZ}(\mathbf{k}) = 0$ elsewhere. This is because for each $\mathbf{k}-\mathbf{k}'+\mathbf{G}$ there is exactly one $\mathbf{G}'$ that reduces $\mathbf{k}-\mathbf{k}'+\mathbf{G}$ to the first BZ.

In a similar way, we obtain for the modulated hopping Hamiltonian from Eq. (11),

$$H_{\rm MH} = -\frac{1}{\sqrt{A}} \sum_{\substack{\mathbf{k}\mathbf{k}'\epsilon BZ \\ ss'\sigma\mu}} \left(\frac{\hbar A_0}{2M_c a^2 \omega^\mu_{\mathbf{k}-\mathbf{k}'}}\right)^{1/2} \frac{4}{3} D_{\rm MH} W_\mu^{\rm MH}(\mathbf{k}s,\mathbf{k}'s') \times [d^\dagger_{-\mathbf{k}+\mathbf{k}',\mu} + d_{\mathbf{k}-\mathbf{k}',\mu}] c^\dagger_{\mathbf{k}s\sigma} c_{\mathbf{k}'s'\sigma},$$

where

$$W_\mu^{\rm MH}(\mathbf{k}s,\mathbf{k}'s') = \frac{i}{2}[s e^{i\phi(\mathbf{k})}(\mathbf{F}(-\mathbf{k})\cdot\vec{\eta}_{\mu 1}(\mathbf{q}) - \mathbf{F}(-\mathbf{k}')\cdot\vec{\eta}_{\mu 2}(\mathbf{q}) e^{-i\mathbf{G}_u\cdot\vec{\delta}_1}) + s' e^{-i\phi(\mathbf{k}')}(\mathbf{F}(\mathbf{k}')\cdot\vec{\eta}_{\mu 1}(\mathbf{q}) - \mathbf{F}(\mathbf{k})\cdot\vec{\eta}_{\mu 2}(\mathbf{q}) e^{-i\mathbf{G}_u\cdot\vec{\delta}_1})] \tag{24}$$

with $\mathbf{q}$ and $\mathbf{G}_u$ defined below Eq. (21). The function $\mathbf{F}(\mathbf{k})$ is defined by

$$\mathbf{F}(\mathbf{k}) = \frac{1}{a}\sum_{j=1}^{3} \vec{\delta}_j e^{i\mathbf{k}\cdot\vec{\delta}_j}, \tag{25}$$

which in our choice of coordinate system yields

$$\mathbf{F}(\mathbf{k}) = [e^{i\frac{1}{2}k_x a}\cos(\sqrt{3}k_y a/2) - e^{-ik_x a}]\hat{x} + [i\sqrt{3}e^{i\frac{1}{2}k_x a}\sin(\sqrt{3}k_y a/2)]\hat{y}.$$

We note again that the deformation potential strength $W_\mu^{\rm DP}(\mathbf{k}s,\mathbf{k}'s')$ in Eq. (21) contains a sum over reciprocal lattice vectors **G** and therefore requires a physical cutoff in wave vector space, provided by the finite range of the interaction W. In contrast, the modulated hopping strength $W_\mu^{\rm MH}(\mathbf{k}s,\mathbf{k}'s')$ in Eq. (24) involves only regular umklapp processes with wavevectors that are within the first Brillouin zone, and at most a reciprocal lattice vector that reduces $\mathbf{q} = \mathbf{k}-\mathbf{k}'$ to the first BZ, with $\mathbf{k}$ and $\mathbf{k}'$ restricted to the first BZ.

The total electron-phonon Hamiltonian is now of the form

$$H_{\rm MH} + H_{\rm DP} = \frac{1}{\sqrt{A}} \sum_{\substack{\mathbf{k}\mathbf{k}'\epsilon BZ \\ ss'\sigma\mu}} \left(\frac{\hbar A_0}{2M_c a^2 \omega^\mu_{\mathbf{k}-\mathbf{k}'}}\right)^{1/2} M_\mu(\mathbf{k}s,\mathbf{k}'s') \times [d^\dagger_{-\mathbf{k}+\mathbf{k}',\mu} + d_{\mathbf{k}-\mathbf{k}',\mu}] c^\dagger_{\mathbf{k}s\sigma} c_{\mathbf{k}'s'\sigma}$$

with the transition matrix element

$$M_\mu(\mathbf{k}s,\mathbf{k}'s') = -\frac{4}{3} D_{\rm MH} W_\mu^{\rm MH}(\mathbf{k}s,\mathbf{k}'s') - D_{\rm DP} W_\mu^{\rm DP}(\mathbf{k}s,\mathbf{k}'s'). \tag{26}$$

Straightforward evaluation of the diagrams for the lowest (second-order) electron self-energy, shown in Fig. 2, and applying the quasiparticle approximation $\Sigma_s(\mathbf{k}) = \Sigma_s(\mathbf{k},\hbar\omega = E_s^{(0)}(\mathbf{k}))$, yields

$$\Sigma_s(\mathbf{k}) = \frac{1}{A}\sum_{\mathbf{k}'\in{\rm BZ},\mu s'} C^\mu_{s,s'}(\mathbf{k},\mathbf{k}') \times \left[\frac{1 - f_{s'}(\mathbf{k}') + n^{\rm ph}_\mu(\mathbf{k}-\mathbf{k}')}{E_s^{(0)}(\mathbf{k}) - E_{s'}^{(0)}(\mathbf{k}') - \hbar\omega^\mu_{\mathbf{k}-\mathbf{k}'} + i\zeta} + \frac{f_{s'}(\mathbf{k}') + n^{\rm ph}_\mu(\mathbf{k}'-\mathbf{k})}{E_s^{(0)}(\mathbf{k}) - E_{s'}^{(0)}(\mathbf{k}') + \hbar\omega^\mu_{\mathbf{k}'-\mathbf{k}} + i\zeta}\right], \tag{27}$$

with $(1/A)\sum_{\mathbf{k}'\in BZ} = \int_{\rm BZ} d^2k'/(2\pi)^2$, ζ is a small positive constant ensuring the retarded nature of the self-energy, and the coupling coefficients (squared transition matrix elements)

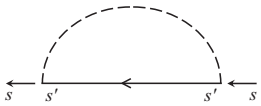

FIG. 2. Feynman diagram for e-ph interaction; intraband (interband) contributions $s = s'(s \neq s')$; dashed line = phonon Green's function.

are

$$C^{\mu}_{s,s'}(\mathbf{k},\mathbf{k}') = \frac{\hbar}{2M_c a^2}\frac{A_o}{\omega^{\mu}_{\mathbf{k}-\mathbf{k}'}}\left|\frac{4}{3}D_{\mathrm{MH}}W^{\mathrm{MH}}_{\mu}(\mathbf{k}s,\mathbf{k}'s') + D_{\mathrm{DP}}W^{\mathrm{DP}}_{\mu}(\mathbf{k}s,\mathbf{k}'s')\right|^2. \quad (28)$$

The self-energy contains intraband ($s = s'$) and interband contributions ($s \neq s'$). The electronic distributions functions are denoted by $f_s(\mathbf{k})$, and $n^{\mathrm{ph}}_{\mu}(\mathbf{k}) = 1/(e^{\hbar\omega^{\mu}_{\mathbf{k}}/k_BT} - 1)$ is the Bose function for the phonons.

We note that for acoustic branches, where $\omega^{\mu}_{\mathbf{Q}} \to 0$ linearly in $\mathbf{Q} = \mathbf{k} - \mathbf{k}'$, the deformation potential contribution to $C^{\mu}_{s,s'}(\mathbf{k},\mathbf{k}')$ has terms of the form $(\mathbf{Q} - \mathbf{G})/\omega^{\mu}_{\mathbf{Q}}$. In the first BZ for which $\mathbf{G} = \mathbf{0}$, this limit is trivially without singularities. In all other Brillouin zones, where $\mathbf{G} \neq \mathbf{0}$, the absence of singularities is not obvious. We address this issue in Appendix C.

The electron-phonon self-energy (e.g., Refs. [35,50,51,93,94]) $\Sigma_s(\mathbf{k})$ critically contributes to many physical observables such as electrical conductivity and optical spectra. Electrical conductivity is largely determined by scattering processes close to the Dirac point. However, optical techniques provide tools for studying electron phonon interactions at a variety of points in the Brillouin zone, so knowledge of $\Sigma_s(\mathbf{k})$ over the entire Brillouin zone becomes more important. In an ultrafast spectroscopic differential transmission investigation of transitions close to the M point, recent studies of nonlinear optical processes involved the differential self-energy $\Delta\Sigma_s(\mathbf{k})$, defined by

$$\Delta\Sigma_s(\mathbf{k}) = \frac{1}{A}\sum_{\mathbf{k}'\in\mathrm{BZ},\mu s\prime} C^{\mu}_{s,s\prime}(\mathbf{k},\mathbf{k}') \times\left[\frac{-\Delta f_{s'}(\mathbf{k}') + \Delta n^{\mathrm{ph}}_{\mu}(\mathbf{k}-\mathbf{k}')}{E^{(0)}_s(\mathbf{k}) - E^{(0)}_{s'}(\mathbf{k}') - \hbar\omega^{\mu}_{\mathbf{k}-\mathbf{k}'} + i\zeta} + \frac{\Delta f_{s'}(\mathbf{k}') + \Delta n^{\mathrm{ph}}_{\mu}(\mathbf{k}'-\mathbf{k})}{E^{(0)}_s(\mathbf{k}) - E^{(0)}_{s'}(\mathbf{k}') + \hbar\omega^{\mu}_{\mathbf{k}'-\mathbf{k}} + i\zeta}\right], \quad (29)$$

where $\Delta f_s(\mathbf{k})$ and $\Delta n^{\mathrm{ph}}_{\mu}(\mathbf{k})$ denote the optically induced changes to the electronic and phonon distribution functions. [Note that we do not calculate the self-energy self-consistently, but rather we depend on unrenormalized band energies $E^{(0)}_s(\mathbf{k})$.] In Sec. IV, we present a numerical study of the electron-phonon self-energy $\Sigma_s(\mathbf{k})$, the differential self-energy $\Delta\Sigma_s(\mathbf{k})$, and the coefficients $C^{\mu}_{s,s'}(\mathbf{k},\mathbf{k}')$, which determine the strength of scattering an electron from initial state $\mathbf{k}',s'$ to final state $\mathbf{k},s$ via electron-phonon interaction involving phonons from branch μ.

III. LIMITING EXPRESSIONS CLOSE TO DIRAC POINT

To validate the appropriateness of this methodology, we first use it to calculate the scattering strengths $W^{\mathrm{MH}}_{\mu}(\mathbf{k}s,\mathbf{k}'s')$ and $W^{\mathrm{DP}}_{\mu}(\mathbf{k}s,\mathbf{k}'s')$ close to the Dirac K point and compare the results with the published literature. We believe this is useful because the expressions depend on the choice of the coordinate system and hence are not exactly the same as, for example, in Ref. [53]. Furthermore, when comparing our results with the results in Refs. [53], we identify the relative sign of the deformation potentials D_{MH} and D_{DP} that enter the coupling coefficient $C^{\mu}_{s,s'}(\mathbf{k},\mathbf{k}')$ (i.e., the squared transition matrix element) given in Eq. (28). We also identify our deformation potential parameters with those in Ref. [55], and we will comment on the concept of effective deformation potentials.

We write $\mathbf{k} = \mathbf{K} + \mathbf{p}$ and $\mathbf{k}' = \mathbf{K} + \mathbf{p}'$, where $\mathbf{K}$ denotes the Dirac point and $\mathbf{p}$ ($\mathbf{p}'$) are small deviations from the Dirac point. We denote by $\theta_{\mathbf{p}}$ the angle of the vector $\mathbf{p}$ relative to the x axis in the two-dimensional plane, and similarly for $\mathbf{p}'$ and $\mathbf{q}$ with $\mathbf{q} = \mathbf{p} - \mathbf{p}'$. We expand the scattering strengths and other quantities to leading order in $q = |\mathbf{q}|$. For the phase in Eq. (18), we obtain $\phi(\mathbf{k}) = \theta_{\mathbf{p}} - \theta_{\mathbf{K}} + \pi$ in the vicinity of the Dirac point $\mathbf{K} = \frac{2\pi}{3a}(1, 1/\sqrt{3})$ with $\theta_{\mathbf{K}} = 30^{\circ}$, and similarly $\phi(\mathbf{k}) = -\theta_{\mathbf{p}} + \theta_{\mathbf{K}'} + \pi$ in the vicinity of the Dirac point $\mathbf{K}' = \frac{2\pi}{3a}(1, -1/\sqrt{3})$.

For the intraband coupling, we find for the acoustical phonon contributions

$$W^{\mathrm{MH}}_{\mathrm{TA}}(\mathbf{K}+\mathbf{p},1;\mathbf{K}+\mathbf{p}',1) = \frac{3aq}{4\sqrt{2}}e^{i\frac{1}{2}(\theta_{\mathbf{p}}-\theta_{\mathbf{p}'})}\cos\frac{1}{2}(\theta_{\mathbf{p}} + \theta_{\mathbf{p}'} + 4\theta_{\mathbf{q}}), \quad (30)$$

$$W^{\mathrm{MH}}_{\mathrm{LA}}(\mathbf{K}+\mathbf{p},1;\mathbf{K}+\mathbf{p}',1) = \frac{3aq}{4\sqrt{2}}e^{i\frac{1}{2}(\theta_{\mathbf{p}}-\theta_{\mathbf{p}'})}\sin\frac{1}{2}(\theta_{\mathbf{p}} + \theta_{\mathbf{p}'} + 4\theta_{\mathbf{q}}), \quad (31)$$

$$W^{\mathrm{DP}}_{\mathrm{LA}}(\mathbf{K}+\mathbf{p},1;\mathbf{K}+\mathbf{p}',1) = \frac{aq}{\sqrt{2}}e^{i\frac{1}{2}(\theta_{\mathbf{p}}-\theta_{\mathbf{p}'})}\cos\frac{1}{2}(\theta_{\mathbf{p}} - \theta_{\mathbf{p}'}), \quad (32)$$

and for the optical phonon contributions

$$W^{\mathrm{MH}}_{\mathrm{LO}}(\mathbf{K}+\mathbf{p},1;\mathbf{K}+\mathbf{p}',1) = -\frac{3i}{\sqrt{2}}e^{i\frac{1}{2}(\theta_{\mathbf{p}}-\theta_{\mathbf{p}'})}\sin\frac{1}{2}(\theta_{\mathbf{p}} + \theta_{\mathbf{p}'} + 2\theta_{\mathbf{q}}), \quad (33)$$

$$W^{\mathrm{MH}}_{\mathrm{TO}}(\mathbf{K}+\mathbf{p},1;\mathbf{K}+\mathbf{p}',1) = \frac{3i}{\sqrt{2}}e^{i\frac{1}{2}(\theta_{\mathbf{p}}-\theta_{\mathbf{p}'})}\cos\frac{1}{2}(\theta_{\mathbf{p}} + \theta_{\mathbf{p}'} + 2\theta_{\mathbf{q}}), \quad (34)$$

$$W^{\mathrm{DP}}_{\mathrm{LO}}(\mathbf{K}+\mathbf{p},1;\mathbf{K}+\mathbf{p}',1) = \mathcal{O}(q^2). \quad (35)$$

Note that there is no deformation potential contribution to transverse phonon modes, as a result of the dot product found in Eq. (20).

For the general expression including interband and intraband couplings, we have for the acoustical phonon

contributions

$$W_{\mathrm{TA}}^{\mathrm{MH}}(\mathbf{K}+\mathbf{p},s;\mathbf{K}+\mathbf{p}',s') = \frac{3aq}{8\sqrt{2}}[se^{i(\theta_{\mathbf{p}}+2\theta_{\mathbf{q}})} + s'e^{-i(\theta_{\mathbf{p}'}+2\theta_{\mathbf{q}})}], \tag{36}$$

$$W_{\mathrm{LA}}^{\mathrm{MH}}(\mathbf{K}+\mathbf{p},s;\mathbf{K}+\mathbf{p}',s') = -i\frac{3aq}{8\sqrt{2}}[se^{i(\theta_{\mathbf{p}}+2\theta_{\mathbf{q}})} - s'e^{-i(\theta_{\mathbf{p}'}+2\theta_{\mathbf{q}})}], \tag{37}$$

$$W_{\mathrm{LA}}^{\mathrm{DP}}(\mathbf{K}+\mathbf{p},s;\mathbf{K}+\mathbf{p}',s') = \frac{aq}{2\sqrt{2}}[1+ss'e^{i(\theta_{\mathbf{p}}-\theta_{\mathbf{p}'})}], \tag{38}$$

and for the optical phonon contributions

$$W_{\mathrm{LO}}^{\mathrm{MH}}(\mathbf{K}+\mathbf{p},s;\mathbf{K}+\mathbf{p}',s') = -\frac{3}{2\sqrt{2}}[se^{i(\theta_{\mathbf{p}}-\theta_{\mathbf{q}})} - s'e^{-i(\theta_{\mathbf{p}'}-\theta_{\mathbf{q}})}], \tag{39}$$

$$W_{\mathrm{TO}}^{\mathrm{MH}}(\mathbf{K}+\mathbf{p},s;\mathbf{K}+\mathbf{p}',s') = \frac{3i}{2\sqrt{2}}[se^{i(\theta_{\mathbf{p}}-\theta_{\mathbf{q}})} + s'e^{-i(\theta_{\mathbf{p}'}-\theta_{\mathbf{q}})}], \tag{40}$$

$$W_{\mathrm{LO}}^{\mathrm{DP}}(\mathbf{K}+\mathbf{p},s;\mathbf{K}+\mathbf{p}',s') = \mathcal{O}(q^2). \tag{41}$$

Using these expressions, we can relate the parameters D_{MH} and D_{DP} derived here with similar parameters from the literature. For LA phonons, our intraband coupling coefficient close to the Dirac point is

$$C_{1,1}^{\mathrm{LA}}(\mathbf{k},\mathbf{k}') = \frac{\hbar}{4M_c}\frac{A_o}{\omega_{\mathbf{q}}^{\mathrm{LA}}}q^2\left|D_{\mathrm{MH}}\sin\frac{1}{2}(\theta_{\mathbf{p}}+\theta_{\mathbf{p}'}+4\theta_{\mathbf{q}}) + D_{\mathrm{DP}}\cos\frac{1}{2}(\theta_{\mathbf{p}}-\theta_{\mathbf{p}'})\right|^2. \tag{42}$$

For comparison with Kaasbjerg *et al.*, Ref. [53], we combine Eqs. (5) and (7) of that paper, square them, and obtain, using the notation in their paper,

$$\left|g_{\mathbf{kq}}^{\mathrm{LA}}\right|^2 = \frac{\hbar}{2A\rho\omega_{\mathbf{q}LA}}q^2\left|\beta\cos\left(2\theta_{\mathbf{q}}+\frac{1}{2}(\theta_{\mathbf{k}}+\theta_{\mathbf{k}+\mathbf{q}})\right) + \alpha\cos\frac{1}{2}(\theta_{\mathbf{k}+\mathbf{q}}-\theta_{\mathbf{k}})\right|^2. \tag{43}$$

We use $\rho = 2M_c/A_0$ for the mass density and assume the extra factor $1/A$ in Eq. (43) corresponds to the same factor we have in Eq. (27). The first term in Eq. (42) is $\sin(2\theta_{\mathbf{q}} + \frac{1}{2}(\theta_{\mathbf{p}}+\theta_{\mathbf{p}'}))$, while that in Eq. (43) is $\cos(2\theta_{\mathbf{q}} + \frac{1}{2}(\theta_{\mathbf{k}}+\theta_{\mathbf{k}+\mathbf{q}}))$. The values of these angles depend on the choice of the reference direction relative to which the angles are defined. For example, a rotation of the reference axis by 30° would convert the sine function in question into a cosine. We suspect the apparent difference of sine and cosine in Eqs. (42) and (43) could be nothing more than a difference in the coordinate convention. Therefore, with this caveat we can make the following assignment:

$$D_{\mathrm{DP}} = \alpha, \tag{44}$$

$$D_{\mathrm{MH}} = \beta. \tag{45}$$

In order to determine the relative sign between D_{MH} and D_{DP}, we plot in Fig. 3 our matrix element [compare Eq. (28)] as $\frac{\sqrt{2}}{a}|\frac{4}{3}D_{\mathrm{MH}}W^{\mathrm{MH}} + D_{\mathrm{DP}}W^{\mathrm{DP}}|$ for comparison with Fig. 1 of Ref. [53], using $D_{\mathrm{MH}} = \pm 2.5$ eV and $D_{\mathrm{DP}} = -2.8$ eV

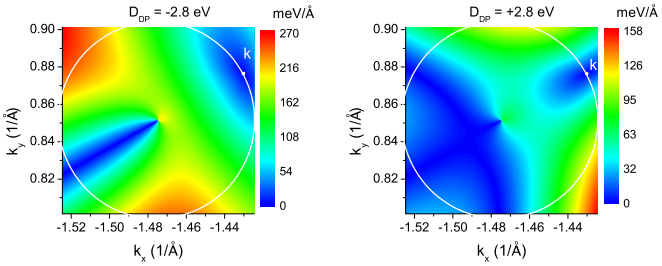

FIG. 3. The squared matrix element from Eq. (43) in the vicinity of the Dirac point with $D_{\mathrm{MH}} = -2.5$ eV and $D_{\mathrm{DP}} = \pm 2.8$ eV (− left, + right) for comparison with Fig. 1 of Ref. [53]. The case of both deformation potentials being negative (left) yields the same structure as in Ref. [53].

where, as pointed out in Sec. II A, D_{MH} is assumed to be negative. We obtain good agreement with Ref. [53] only for $D_{\mathrm{MH}} = -2.5$ eV, while opposite signs of D_{MH} and D_{DP} do not reproduce the DFT results in Ref. [53]. (Again, note that in our geometry, the hexagons in k space include vertical lines, whereas in Kaasbjerg's geometry they include horizontal lines, explaining the relative rotation of our Fig. 3 to Kaasbjerg's Fig. 1.)

We next compare our expressions with those given in Park *et al.*, Ref. [55] as follows. Squaring the LA coupling matrix element from Table I of Ref. [55], we have, using their notation (the symbol η in Ref. [55] should not be confused with the displacement vectors $\vec{\eta}$ used throughout this paper),

$$\left|g_{1,1}^{\mathrm{LA}}(\mathbf{p},\mathbf{q})\right|^2 = \frac{\hbar|\mathbf{k}'-\mathbf{k}|}{4M_c v_s^{\mathrm{LA}}}\left|\frac{3}{4}b\eta\cos\left(2\theta_{\mathbf{k}'-\mathbf{k}}+\frac{1}{2}(\theta_{\mathbf{k}}+\theta_{\mathbf{k}'})\right) + D\cos\frac{1}{2}(\theta_{\mathbf{k}}-\theta_{\mathbf{k}'})\right|^2. \tag{46}$$

Here, $\omega_{\mathbf{q}}^{\mathrm{LA}} = v_s^{\mathrm{LA}}q$ and $|\mathbf{k}'-\mathbf{k}| = q$, and we assume that their expression must be multiplied by A_0 in order to compare with ours. This latter assumption is based on the fact that the k' integral in our self-energy involves $\int_{\mathrm{BZ}} d^2k'/(2\pi)^2$, see Eq. (27), whereas in much of the literature, it is written as $\int_{\mathrm{BZ}} d^2k'/A_{\mathrm{BZ}}$, where $A_{\mathrm{BZ}} = (2\pi)^2/A_0$ is the area of the Brillouin zone, see, for example, Eq. (17) of Ref. [51]. With this, we find the following association between our parameters and those of Ref. [55]:

$$D_{\mathrm{MH}} = \tfrac{3}{4}b\eta, \tag{47}$$

$$D_{\mathrm{DP}} = D. \tag{48}$$

In Ref. [55], the conventional deformation potential was set to zero ($D = 0$) and $\eta = 4.57$ eV/Å, $b = 1.405$ Å, giving $\frac{3}{4}b\eta \simeq 5$ eV, slightly larger but roughly the same order of magnitude than the value $\beta_{\mathrm{LA}} = 2.5$ eV in Ref. [53]. See Ref. [55] for a discussion of that difference.

We finally would like to comment on the concept of so-called effective deformation potentials, a formalism in which contributions from modulated hopping (with longitudinal and transverse phonons) are absorbed in the conventional (longitudinal phonon) deformation potential terms. This means

that the angular dependence of the electron phonon coupling is assumed to be that of the conventional deformation potential, whereas the numerical value of the conventional deformation potential is adjusted in a way that it approximately includes the modulated hopping contribution. This concept has been used for scattering involving acoustical and optical phonons. For example, Ref. [53] introduces an effective deformation potential $\Xi \simeq 5$ eV for electron-acoustic phonon scattering, using the simple isotropic angular dependence of Eq. (32), rather than using the more complex, anisotropic angular dependence of Eqs. (30) and (31).

In our recent study, Ref. [61], we adopted that concept and found good agreement with our experimental pump-probe measurements near the M point. Similarly, an optical deformation potential was used in Ref. [71] with a value of 11 eV/Å using an angular dependence based on the form given in Eq. (32). In Ref. [61], we adopted the concept of an effective optical deformation potential with the angular dependence of the conventional longitudinal acoustical deformation potential coupling and a value of $D^{\rm op}_{\rm eff} = 11$ eV/Å. We found reasonable agreement with the experiment, but the theoretical values for the differential transmission were slightly larger than those obtained from the experiment.

In order to introduce an effective optical deformation potential using the expressions $W^{\rm MH}_{\mu}(\mathbf{k}s,\mathbf{k}'s')$ given above, we introduce an effective optical deformation by using Eq. (33):

$$C^{\rm LO}_{1,1}(\mathbf{k},\mathbf{k}') = \frac{\hbar A_o}{4M_c\omega^{\rm LO}_{\mathbf{q}}}\frac{16}{a^2}D^2_{\rm MH}\sin^2\frac{1}{2}(\theta_{\mathbf{p}}+\theta_{\mathbf{p}'}+2\theta_{\mathbf{q}}). \quad (49)$$

Constructing now an effective optical coupling by replacing the anisotropic angular dependence by the isotropic form,

$$C^{\rm op}_{\rm eff}(\mathbf{k},\mathbf{k}') = \frac{\hbar A_o}{4M_c\omega^{\rm LO}_{\mathbf{q}}}D^2_{\rm op,eff}\cos^2\frac{1}{2}(\theta_{\mathbf{p}}-\theta_{\mathbf{p}'}), \quad (50)$$

we have $D_{\rm op,eff} = 4D_{\rm MH}/a$. Using the above value of $D_{\rm MH} = 2.5$ eV, and $a = 1.42$ Å, we find $D_{\rm op,eff} = 7$ eV/Å, which would improve our agreement with the experiment. However, rather than using effective deformation potential models, in this paper, we present results using the full model given by Eq. (28).

IV. NUMERICAL RESULTS FOR TRANSITION MATRIX ELEMENTS AND SELF-ENERGIES FOR THE ENTIRE BZ

In this section, we present a numerical analysis of the transition matrix elements and self-energies. We do not restrict ourselves to results close to the Dirac point, but show results for the entire BZ. We numerically solve Eq. (28) for the squared transition matrix elements (i.e., the probabilities for electron scattering from $\mathbf{k}',s'$ to $\mathbf{k},s$) and the corresponding electronic self-energy Eq. (27), which determines, among other things, transport coefficients, and the differential self-energy Eq. (29), which determine the optical differential transmission signal. The phonon eigenvalues and eigenvectors entering the $C^{\mu}_{s,s'}(\mathbf{k},\mathbf{k}')$ are calculated as shown in Appendix B. Unless otherwise noted, we use $D_{\rm MH} = -2.5$ eV, $D_{\rm DP} = -2.8$ eV, $a = 1.42$ Å, $t_0 = 2.55$ eV, temperature $T = 300$ K, and $\zeta = 50$ meV, a value small compared to the energy scale

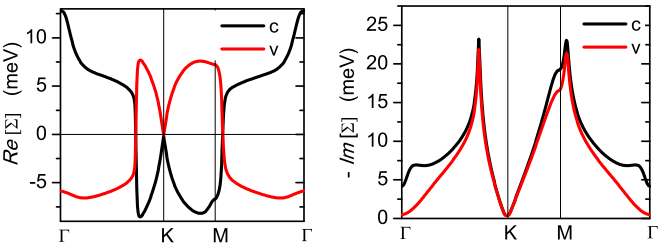

FIG. 4. Self-energy (left: real part, right: imaginary part times -1) at temperature $T = 300$ K including both deformation potential (DP) and modulated hopping (MH) contributions for the conduction (c) band, $s = +1$, and valence (v) band, $s = -1$.

in our problem but large enough for the k discretization in the numerical evaluation of the self-energy.

The self-energy is shown in Figs. 4 and 5. The overall features are in accordance with second-order perturbation theory, as pointed out on p. 166 of Ref. [95] (cf. also Ref. [96]). Second-order energy corrections are of the form $E^{(2)}_i = \sum_{j\neq i}|V_{i,j}|^2/(E^{(0)}_i - E^{(0)}_j)$, where $V_{i,j}$ are perturbation matrix elements between states i and j. Neglecting the (small) phonon energy in the denominator, Eq. (27), makes the self-energy structure similar to calculations from conventional perturbation theory. Considering first the conduction (c band, $s = +1$) band in Eq. (27), we have a subset of energies with lower and upper bound, and the expression for $E^{(2)}_i$ shows that the shift of the lower (upper) bound is negative (positive). We see from Fig. 4 that indeed the shift (real part of Σ) is positive at the highest c-band energy (i.e., at Γ), and negative at the smallest c-band energy (i.e., at K). In Fig. 4, we see that the real part of Σ changes sign slightly above the M point. The Kramers-Kronig relations dictate that there is a peak in the imaginary part of Σ close to where the real part changes sign, as seen in Fig. 4. A similar discussion holds for the valence (v band, $s = -1$) band, except that the highest energy is at the K point and the lowest at Γ. These features also hold qualitatively for the differential self-energy Eq. (29).

We see from Fig. 4 that the real part of the c- and v-band self-energy becomes very small at the Dirac point. To analyze this behavior further, we show in Fig. 6 the intra (cc) and inter (cv) contributions. For semiconductors like GaAs, which have a gap, it is not uncommon to restrict calculations of the electron self-energy due to electron-phonon coupling to just intraband contributions: the interband contributions are small

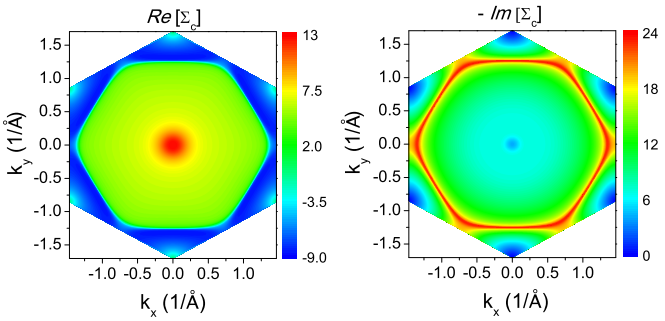

FIG. 5. Same as Fig. 4 but as a contour plot for the conduction-band component Σ_c (or $s = +1$). Units are meV.

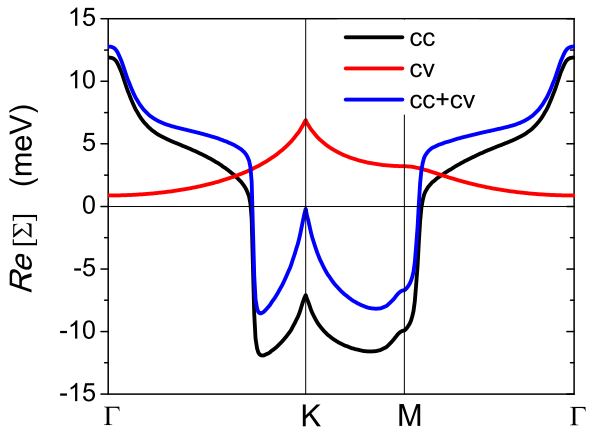

FIG. 6. The real part of the interband (cv) contribution to the self-energy exists throughout the BZ. Close to the K point, it cancels to a high degree the intraband (cc) contribution.

due to the appearance of the gap in the energy denominator. For graphene, however, that would not be appropriate. From Fig. 6, we see that there is a strong cancellation between intra- and interband contributions that becomes gradually more perfect as we approach the K point. Indeed, if the conical intersection of c and v bands, characteristic for graphene, is to be preserved by electron-phonon interaction, then either both c and v self-energies have to vanish at K, or both have to be equal (i.e., they cannot have opposite signs). The former is the case for $T = 0$ K, and the latter has been found to be true in Ref. [50]. We also note that the imaginary part of the interband self-energy (not shown) is very small except very close to K, as the transition energies from v to c are much larger than the phonon energies.

Another feature of Fig. 4 is the lack of electron-hole symmetry of the form $\Sigma_v(\mathbf{k}) = -\Sigma_c^*(\mathbf{k})$. The symmetric two-band model employed here preserves electron-hole symmetry in the sense that $E_v(\mathbf{k}) = -E_c(\mathbf{k})$. At $T = 0$ K, the electron-hole symmetry is also preserved by the distribution functions, and at nonzero temperature the symmetry is preserved approximately, $f_v(\mathbf{k}) \simeq 1 - f_c(\mathbf{k})$. (Note that we do not consider doped graphene.) The reason for the breaking of the electron-hole symmetry seen in Fig. 4 is related to the squared matrix elements (*i.e.* coupling coefficients). If we had either DP or MH, but not both, the symmetry would still be preserved, $C^{\mu}_{cc}(\mathbf{k},\mathbf{k}') = C^{\mu}_{vv}(\mathbf{k},\mathbf{k}')$. But the DP and MH couplings add up coherently in Eq. (28), and they have different behavior under c-to-v exchange (MH changes sign, while DP does not). Thus the coherent superposition of DP and MH scattering leads to a breaking of the electron-hole symmetry.

Next, we take a more detailed look at the coupling coefficients. In Fig. 7, we show the result for the sum of LA plus LO phonon contributions for three choices of $\mathbf{k}$. The DP coupling has a finite range in k space; it is restricted to small wave vector transfers $\mathbf{q} = \mathbf{k} - \mathbf{k}'$, as discussed in Appendix A. For $\mathbf{k}$ at the Dirac (here K') or M point, we see DP scattering at the opposite side of the BZ, which indicates umklapp processes that are discussed in Sec. V. Unlike scattering via DP, scattering via MH is not restrictive to the vicinity of $\mathbf{k}$ and is relatively strong across the entire BZ. For $\mathbf{k}$ at Γ, it is very weak, while $\mathbf{k}$ at M it dominates for small wave vector

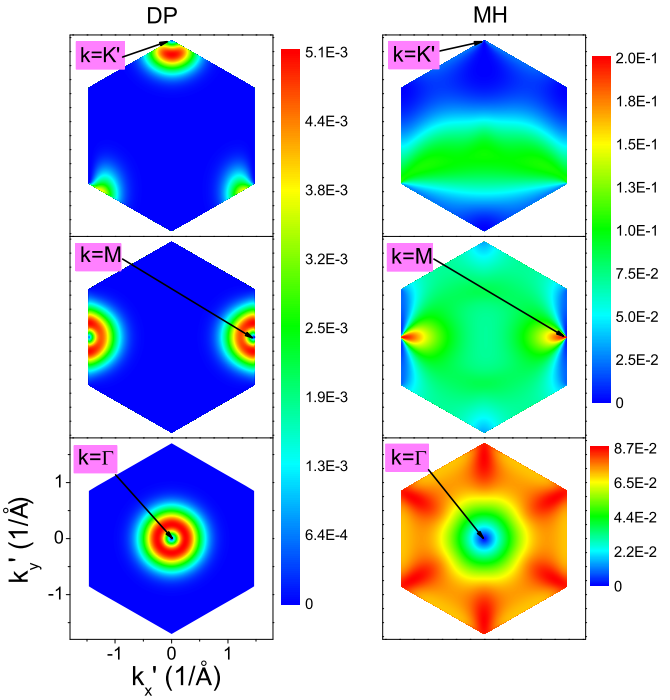

FIG. 7. The squared matrix elements $C^{\mu}_{cc}(\mathbf{k},\mathbf{k}')$ in units of eV^2 Å^2 for fixed $\mathbf{k}$ as a function of $\mathbf{k}'$, for DP (left) and MH (right) contributions. Here the sum $C^{\mathrm{LA}} + C^{\mathrm{LO}}$ is shown.

transfers. Again, umklapp processes exist at the opposite side of the BZ.

We show in Fig. 7 the sum LA plus LO contributions, because each contribution individually features discontinuities, as shown in Fig. 8. The discontinuities are not unphysical but related to the fact the LA and LO phonon frequencies are degenerate on the BZ boundary, which in turn is a result of the equal masses of the two atoms in the basis of the honeycomb lattice. The discontinuities in the electronic self-energies occur at locations that correspond to wave vector transfers $\mathbf{q}$ on the BZ boundary, i.e., the boundary of the phonon dispersion. Crossing that boundary in a continuous way would require going from the LA to the LO branch. If we restrict ourselves to, say, the LA branch, then crossing that boundary involves a discontinuity in the phonon displacement vectors. Since the $C^{\mu}_{cc}(\mathbf{k},\mathbf{k}')$ are in principle physically observable, one might be led to conclude that such discontinuities should also be observable. However, that would require an experimental

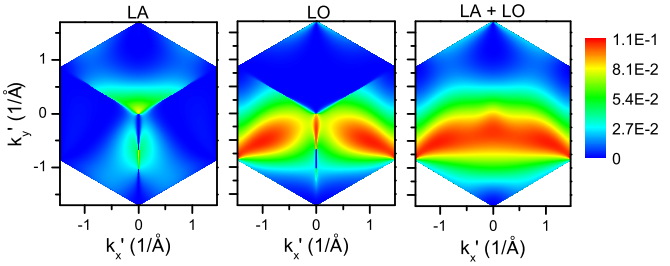

FIG. 8. The MH contribution to $C^{\mu}_{cc}(\mathbf{k},\mathbf{k}')$ in units of eV^2 Å^2 for $\mathbf{k}$ at the K point, showing the individual contributions from LA and LO phonons as well as their sum.

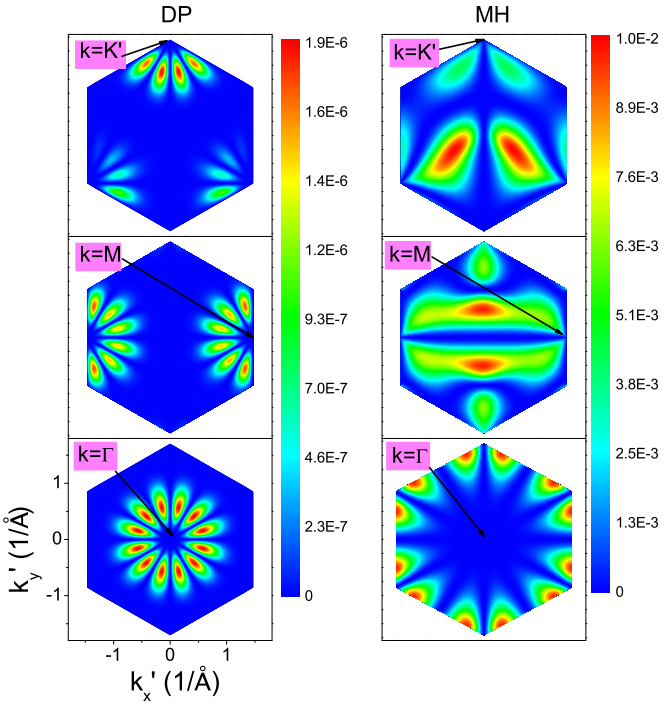

FIG. 9. Same as Fig. 7, but for TA phonons.

restriction to, say, the LA branch, which seems unlikely to be realizable.

Figures 9 and 10 show the squared matrix elements due to TA and TO phonons, respectively. The DP scattering through coupling to the transverse phonons is weak. In textbook treatments, this contribution is often completely neglected, as in the long-wavelength limit the transverse

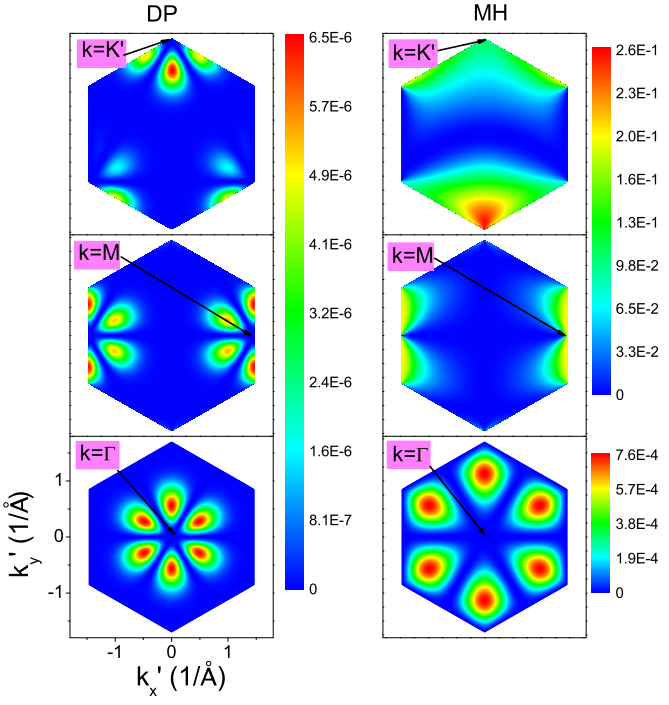

FIG. 10. Same as Fig. 7, but for TO phonons.

phonon displacement vectors are indeed strictly transverse, and a coupling containing a factor $\mathbf{q} \cdot \vec{\eta}$ vanishes. However, on the larger scale of the entire BZ, the displacement vectors deviate from being purely transversal: quite generally, their translation properties in reciprocal space [Eqs. (13) and (14)] impose a hexagonal symmetry (see Appendix B). Without the finite range in k space of the DP coupling, we would see large DP couplings to transversal phonons in the electronic self-energy, at the locations corresponding to the BZ boundary in the wave vector transfer $\mathbf{q}$. However, the finite range cuts that off, and what we see is the interplay between small DP coupling range (favoring small $\mathbf{q}$) and the deviation from purely transverse displacements (favoring large $\mathbf{q}$ on the BZ boundary). As expected, for coupling to transverse phonons the MH contribution is stronger than the DP contribution. The strongest scattering in Figs. 9 and 10 happens for $\mathbf{k}$ at the K point with MH coupling. This is the well-known iTO coupling discussed in Ref. [65]. Our results are also consistent with those found in Ref. [55].

V. NUMERICAL RESULTS FOR DIFFERENTIAL TRANSMISSION SPECTROSCOPY CLOSE TO THE *M* POINT

In this section, we expand our recently published analysis of differential transmission spectroscopy. In Ref. [61], we presented experimental data for nondegenerate differential transmission spectra, obtained for pump-probe delay times from about 4 to 400 ps and spanning optical transitions close to the M point at frequencies from about 3.6 to 5 eV. We also presented a theoretical simulation using effective deformation potentials as defined in Sec. III above. In the following, we present new analysis of the same experimental data, now using the more general theory outlined above using deformation potential coupling (DP) and modulated hopping (MH) with the same values for D_{DP} and D_{MH} as given in the previous sections, taken from Ref. [53].

We calculate the differential spectra the same way as detailed in Supplement Material to Ref. [61] [see Eqs. (6)–(8) of that Supplement Material and the text following those equations for parameter values]; however, the differential self-energies entering the susceptibility here are those obtained with the DP and MH models. In Fig. 11, we see that the present theory gives overall very good agreement with the experiment. The spectra exhibit regions of negative differential transmission, which might be compared to Refs. [35–37,62], but which in our theoretical model follow solely from an increase of the phonon temperature. The change in phonon temperature is manifest in the temperature dependence of $n_{\mu}^{\mathrm{ph}}(\mathbf{k})$ responsible for the $\Delta n_{\mu}^{\mathrm{ph}}(\mathbf{k})$ in Eq. (29). We assume all phonons have the same elevated temperature, identical to the temperature of the electrons, because the shape of the differential signal does not vary substantially over delay times up to 400 ps (see Fig. 3 of Ref. [61]). At such large delay times, phonons have equilibrated with each other—via phonon anharmonicities—and with the electronic system [78].

Breaking down the differential spectra into contributions from DP and MH, we see that both contributions separately give the correct shape of the spectrum: both give the correct zero crossing and approximately the same ratio of the positive

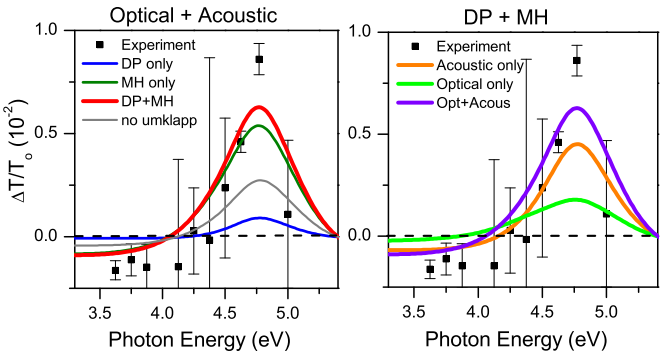

FIG. 11. Calculated differential transmission spectra (solid lines) and experimental data (squares, after Ref. [61], for delay time 4 ps). The equilibrium temperature is 300 K and the elevated phonon temperature is 600 K. (a) The contributions from DP and MH for both optical and acoustic phonons. (b) The contribution from optical and acoustic phonons for DP and MH.

over negative peak values. The absolute contribution of MH is larger than that of DP, but the DP contribution is not negligibly small. Shown in Fig. 11 is also the result without including umklapp processes. It is roughly one half of the full result, which is not surprising given the fact that for transitions close to the M point umklapp processes occupy roughly half of the BZ. A more detailed understanding of the role of umklapp processes is given in Fig. 12. From the definition of umklapp processes, it is clear that scattering processes with wave vector $\mathbf{k}$ fixed at Γ do not involve any umklapp processes: comparing Figs. 7 and 12, we see that there is no region of the BZ missing

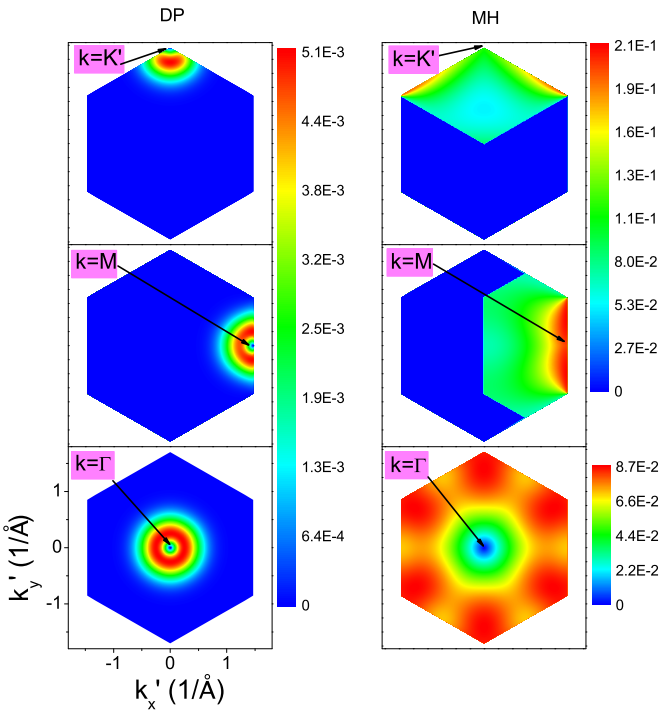

FIG. 12. The squared matrix element, summed over all phonon branches, $\sum_\mu C^\mu_{cc}(\mathbf{k},\mathbf{k}')$ in units of eV^2 Å^2 for fixed $\mathbf{k}$ as a function of $\mathbf{k}'$, for DP (left) and MH (right) contributions, without umklapp processes.

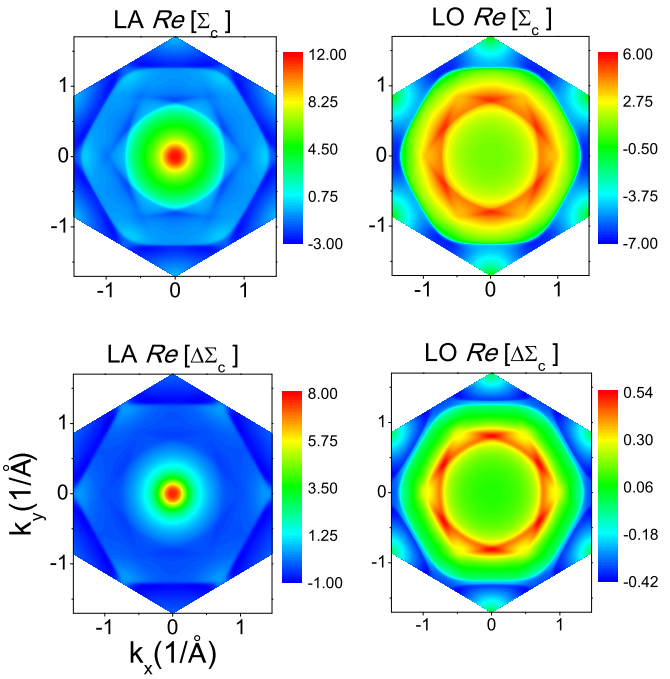

FIG. 13. The longitudinal phonon contributions (LA and LO) to the self-energy (top) and differential self-energy (bottom) in units of meV. The equilibrium temperature is 300 K, and in the differential self-energy, the elevated phonon temperature is 600 K.

due to the omission of umklapp. On the other hand, fixing $\mathbf{k}$ at the M point and omitting umklapp leads to the loss of the contribution from the left side of the BZ. In the case of DP this is almost exactly one half of the scattering processes. For the MH case we see that the area with zero value is actually slightly larger than one half of the BZ.

In Fig. 11, we also break down the total differential transmission into contributions from acoustic and optical phonons. As mentioned above, the acoustic phonons yield a larger contribution than the optical phonons because the differential transmission requires thermal phonon occupation. Note that the differential electronic occupation, $\Delta f_{s'}(\mathbf{k}')$ in Eq. (29), is numerically negligible for the temperatures used in the present case. Hence, while optical phonons often dominate over acoustic phonons, the strength of the acoustic phonons is enhanced in differential transmission measurements. This can also be seen from a global comparison of the underlying self-energies across the BZ, shown in Fig. 13. Comparing the overall magnitudes of the LA and LO self-energies, we see immediately that the approximate maximum values are 12 and 5.5 meV, respectively. In contrast, the differential self-energy yields 7.7 and 0.54 meV, respectively, indicating a much greater role of the acoustic phonons in differential transmission measurements.

VI. CONCLUSIONS

Using an expanded deformation potential approach, we present a theoretical study of the electron-phonon self-energy and scattering matrix elements of graphene across the entire Brillouin zone. With phonon modes obtained from a dynamical

matrix model as input, it is found that both modulated hopping and conventional deformation potentials include umklapp processes, but only deformation potentials require a physical cutoff of its range in reciprocal space. Parameter values for the deformation potential models are obtained from comparison with literature data based on *ab initio* calculations. Discontinuities in the scattering matrix elements inside the electronic BZ are traced to phonon degeneracies at the phonon BZ boundary. We apply the theory to nonlinear optical spectroscopy in the vicinity of the M point and analyze the contribution of umklapp processes to the observable differential transmission signal. We find very good agreement with recently published experimental data.

The use of deformation potentials to parametrize the electron-phonon interaction in graphene is an important tool for the quantitative analysis of transport and optical properties of graphene. The consistency and agreement of our approach with prior work at the Dirac K point and with our ultrafast spectroscopic measurements at the M point indicate the potential of this formalism to explore energy renormalization due to electron-phonon interaction throughout much of the BZ. However, we note that the validity of the theory, which is based on two symmetric bands, likely varies throughout the BZ. Apart from the K point, we have shown that the model is valid close M point (see Sec. V), but close to the Γ point other bands are found in realistic band-structure calculations [97]. These may cause deviations from the predictions of the simple model employed here. Such deviations need to be addressed in future research. Furthermore, the dependence of the deformation potentials D_{MH} and D_{DP} on the substrate is presently not well understood. As discussed in Appendix A, we assume that D_{DP} depends stronger on the choice of substrate than D_{MH}. This assumption should be investigated in future studies. Our present studies may also be helpful for further studies of electron-phonon interaction effects in graphene and other two-dimensional materials, such as the relationship between electron-phonon interactions and topological effects and spin textures in Dirac fermion systems [94,98].

APPENDIX A: MICROSOPIC MOTIVATION OF DEFORMATION POTENTIAL MODEL

Throughout this paper, we use the Hamiltonian (1) as a phenomenological starting point for a theory that includes both conventional deformation potential coupling and modulated hopping coupling. In this appendix, we explore some microscopic motivations that help us understand the functional form of the $\mathbf{q}$-dependent deformation potential coupling and the sign of the deformation potential D_{DP}.

A more general starting point for the derivation of the deformation potential coupling would be that used in text books (e.g., Refs. [83,95]):

$$H_{\text{el-ion}} = -\int n_{\mathrm{el}}(\mathbf{r},\mathbf{z})V(\mathbf{r}-\mathbf{R},z-Z)n_{\mathrm{ion}}(\mathbf{R},Z)d^2r d^2R dz dZ \tag{A1}$$

$$= -\frac{1}{A}\sum_{\mathbf{q}}\int n_{\mathrm{el}}(-\mathbf{q},z)V(\mathbf{q},z-Z)n_{\mathrm{ion}}(\mathbf{q},Z)dz dZ, \tag{A2}$$

where $V(\mathbf{r},z)$ is the Coulomb potential in three dimensions, possibly screened through dielectric screening from the substrate if the graphene layer is attached to a dielectric substrate. The electron (ion) densities are denoted by n_{el} (n_{ion}), and spatial coordinates are denoted by lower case (upper case). In the second line, we performed the two-dimensional Fourier transform ($\mathbf{q} = (q_x,q_y)$) since the graphene layer is extended only in two dimensions. One possible simple way to proceed would be to expand the Coulomb potential in a Taylor series based on the system's small extension in the direction normal to the layer, $V(\mathbf{q},z-Z) \simeq V(\mathbf{q},0) + V'(q,0)(z-Z) + \cdots$, and possibly keeping only the leading order term,

$$V(\mathbf{q},z-Z) \simeq V(\mathbf{q},0). \tag{A3}$$

This approximation is probably more valid at small $\mathbf{q}$ and less appropriate for $\mathbf{q}$ approaching the BZ boundary. Defining the z-integrated electron and ion densities (or their $q_z = 0$ components) via

$$\int n_{\mathrm{el}}(\mathbf{r},z)dz = n_{\mathrm{el}}(\mathbf{r},q_z=0) = n_{\mathrm{el}}(\mathbf{r}),$$

$$\int n_{\mathrm{ion}}(\mathbf{R},Z)dZ = n_{\mathrm{ion}}(\mathbf{R},q_Z=0) = n_{\mathrm{ion}}(\mathbf{R}),$$

the electron-ion interaction becomes

$$H_{\text{el-ion}} = \int n_{\mathrm{el}}(\mathbf{r})V_L(\mathbf{r})d^2r$$

with

$$V_L(\mathbf{r}) = -\int V(\mathbf{r}-\mathbf{R},0)n_{\mathrm{ion}}(\mathbf{R})d^2R.$$

We use the $2p$ wave functions $\Phi_{2p}(\mathbf{r},z)$ for the electron density and the $2s$ functions $\Phi_{2s}(\mathbf{R},Z)$ (highest occupied orbitals) for the ion density, as was done in Ref. [63]. We can then write

$$n_{\mathrm{el}}(\mathbf{r},z) = \sum_{jn\sigma} n_{\mathrm{el}}^{\mathrm{atom}}(\mathbf{r}-\mathbf{R}_{jn},z)c_{jn\sigma}^{\dagger}c_{jn\sigma},$$

with $n_{\mathrm{el}}^{\mathrm{atom}}(\mathbf{r},z) = |\Phi_{2p}(\mathbf{r},z)|^2$, and

$$n_{\mathrm{ion}}(\mathbf{R}) = \sum_{jn} n_{\mathrm{ion}}^{\mathrm{atom}}(\mathbf{R}-\mathbf{R}_{jn})n_{jn}^{\mathrm{ion}},$$

with $n_{\mathrm{ion}}^{\mathrm{atom}}(\mathbf{R}) = \int n_{\mathrm{ion}}^{\mathrm{atom}}(\mathbf{R},Z)\ \mathrm{dZ}$, and $n_{\mathrm{ion}}^{\mathrm{atom}}(\mathbf{R},Z) = Z_e|\Phi_{2s}(\mathbf{R},Z)|^2$, where Z_e is the ion's numeric charge (whose value we do not need to specify as it will be absorbed in the definition of the deformation potential). We can set $n_{jn}^{\mathrm{ion}} = 1$ since in our theory, only small lattice vibrations are allowed, and the number of ions inside each unit cell is always one. Now

$$H_{\text{el-ion}} = \sum_{jn\sigma} V_{jn}c_{jn\sigma}^{\dagger}c_{jn\sigma}$$

with

$$V_{jn} = -\sum_{j'n'}\int n_{\mathrm{el}}^{\mathrm{atom}}(\mathbf{r}-\mathbf{R}_{jn})V(\mathbf{r}-\mathbf{R},0) \times n_{\mathrm{ion}}^{\mathrm{atom}}(\mathbf{R}-\mathbf{R}_{j'n'})n_{j'n'}^{\mathrm{ion}}d^2r d^2R.$$

If we define

$$W(\mathbf{R}_{jn}-\mathbf{R}_{j'n'})=\int n_{\rm el}^{\rm atom}(\mathbf{r}-\mathbf{R}_{jn})V(\mathbf{r}-\mathbf{R},0)\times n_{\rm ion}^{\rm atom}(\mathbf{R}-\mathbf{R}_{j'n'})n_{j'n'}^{\rm ion}d^2rd^2R,$$

we obtain the form that we used in Eqs. (1) and (2):

$$H_{\text{el-ion}}=-\sum_{jn\sigma j'n'}W(\mathbf{R}_{jn}-\mathbf{R}_{j'n'})c_{jn\sigma}^{\dagger}c_{jn\sigma}.$$

Using the two-dimensional Fourier transform, we can write

$$H_{\text{el-ion}}=-\frac{1}{A}\sum_{jn\sigma j'n'\mathbf{q}}e^{i\mathbf{q}\cdot(\mathbf{R}_{jn}^{(0)}-\mathbf{R}_{j'n'}^{(0)})}W(\mathbf{q})c_{jn\sigma}^{\dagger}c_{jn\sigma},\quad\text{(A4)}$$

with $W(\mathbf{q})=n_{\rm el}^{\rm atom}(-\mathbf{q})V(\mathbf{q})n_{\rm ion}^{\rm atom}(\mathbf{q})$.

We follow Ref. [63] and use the following $2p$ and $2s$ model functions: $\Phi_{2p}(\mathbf{r},z)=z/(\sqrt{32\pi a_e^5})e^{-r/(2a_e)}$, and $\Phi_{2s}(\mathbf{r},z)=r/(\sqrt{96\pi a_i^5})e^{-r/(2a_i)}$, where $r=\sqrt{\mathbf{r}^2+z^2}$ and a_e (a_i) is the electron (ion) Bohr radius. These model functions are approximations to the Roothaan-Hartree-Fock wave functions, p. 282 of Ref. [99], where in the $2s$ wave function the r^0 term (i.e., the $1s$ contribution in the Hartree-Fock expansion of the $2s$ wave function) has been neglected because its coefficient is smaller than that of the r^1 terms. The exponential decay constant a_i has been assumed equal for all terms in the Hartree-Fock expansion. We now have

$$n^{\rm atom}(\mathbf{q})=n_{\rm el}^{\rm atom}(-\mathbf{q})n_{\rm ion}^{\rm atom}(\mathbf{q})\quad\text{(A5)}$$

with

$$n_{\rm el}^{\rm atom}(\mathbf{q})=\frac{1}{[1+(qa_e)^2]^3}\quad\text{(A6)}$$

and

$$n_{\rm ion}^{\rm atom}(\mathbf{q})=Z_e\frac{1-(qa_i)^2}{[1+(qa_i)^2]^4}.\quad\text{(A7)}$$

In our numerical calculations, we assume both the electron and the ion Bohr radius to be equal and equal to half of the bond length a, so $a_e=a_i\equiv a_0=a/2$. Clearly, the range of the potential $W(\mathbf{q})$ is limited to values of q not much larger than the inverse bondlength, and therefore roughly constrained to within one Brillouin zone. Because of the strong $\mathbf{q}$-dependence of $n^{\rm atom}(\mathbf{q})$, we assume that for the definition of the $\mathbf{q}$-dependent deformation potential, we can omit the $\mathbf{q}$ dependence of the Coulomb potential. Hence, in our numerical studies, we use

$$D_{\rm DP}(\mathbf{q})=\frac{2}{A_0}W(\mathbf{q})=\frac{2}{A_0}V(\mathbf{0})n^{\rm atom}(\mathbf{q})=D_{\rm DP}\frac{1-(qa_0)^2}{[1+(qa_0)^2]^7},\quad\text{(A8)}$$

with $D_{\rm DP}=2Z_eV(\mathbf{0})/A_0$ and assuming that $V(\mathbf{0})$ is finite. For the case of the two-dimensional screened Coulomb potential,

$$V(\mathbf{q})=\frac{2\pi e^2}{\varepsilon_{\rm eff}[q+\kappa]},\quad\text{(A9)}$$

this requires a nonzero screening length κ, which depends on the amount of plasma screening and therefore on the doping concentration. In Eq. (A9), $\varepsilon_{\rm eff}$ is an effective dielectric screening due to a potential substrate. For example, $\varepsilon_{\rm eff}=(1+\varepsilon_{\rm substrate})/2$ represents the common case of a single graphene layer attached to a substrate (see Refs. [69,74,100]).

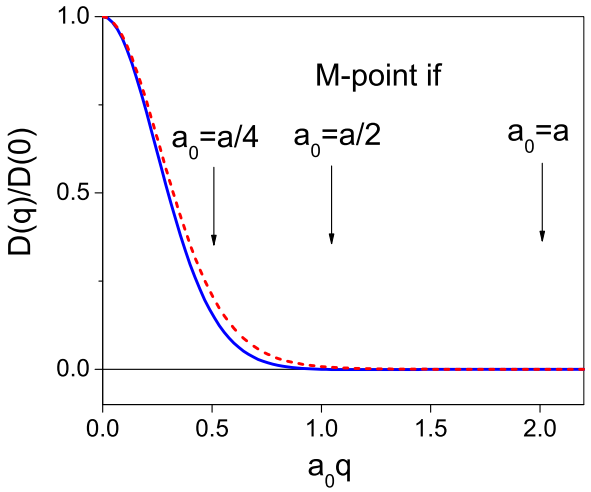

FIG. 14. The q dependence of the deformation potential according to Eqs. (A8) (blue solid line) and (A11) (red dotted line). The position of the M point is indicated for various choices of a_0.

We need to make two remarks regarding this approach. First, based on this approach we would conclude that $D_{\rm DP}=4\pi Z_ee^2/(A_0\varepsilon_{\rm eff}\kappa)$ is positive. Second, $D_{\rm DP}$ depends on the substrate via the factor of $1/\varepsilon_{\rm eff}$. It is then reasonable to assume that the modulated hopping parameter $D_{\rm MH}$ depends less sensitively on the substrate, as it does not carry a factor of $1/\varepsilon_{\rm eff}$. Future experiments that are more sensitive to the conventional deformation potential than the modulated hopping coupling might be able to test whether $D_{\rm DP}$ has indeed a $1/(\varepsilon_{\rm eff})$ dependence.

Regarding the first remark, we note that the possibility of a negative deformation potential can be seen in the expression given by Woods and Mahan [63]. In the notation of their Eq. (49), they give an expression for the deformation potential

$$\widetilde{D}=v(\mathbf{q})\rho_T(\mathbf{q})\rho_e(\mathbf{q})=4\pi Ze^2\left(3\alpha_e^{-2}-5\alpha_i^{-2}\right),\quad\text{(A10)}$$

where $v(\mathbf{q})$ is the Coulomb potential, ρ denotes the densities, and α the inverse Bohr radii. Woods and Mahan introduce a total density $\rho_T(\mathbf{q})=\rho_i(\mathbf{q})-Z\rho_e(\mathbf{q})$, which determines the deformation potential $\widetilde{D}$. For comparison, note that using our notation and the densities given in Eqs. (A6) and (A7) as well as a three-dimensional Coulomb potential $V^{3D}(\mathbf{q})=4\pi e^2/q^2$, the $q\to 0$ limit of $V^{3D}(\mathbf{q})[n_{\rm ion}^{\rm atom}(\mathbf{q})-Z_en_{\rm el}^{\rm atom}(\mathbf{q})]n_{\rm el}^{\rm atom}(\mathbf{q})$ is $4\pi Z_ee^2[3a_e^2-5a_i^2]$. The treatment by Woods and Mahan seems to indicate that a negative deformation potential might be possible. Their $\mathbf{q}$ dependence would be

$$\widetilde{\mathbf{D}}(\mathbf{q})=\widetilde{\mathbf{D}}\frac{1}{[1+(qa_0)^2]^7}\quad\text{(A11)}$$

if again we assume $a_e=a_i=a_0$. For practical purposes, the difference in the q dependence between Eqs. (A8) and (A11) is not large, as shown in Fig. 14. We believe that more studies along the lines outlined in this appendix will be needed in the future to further elucidate the sign and $\mathbf{q}$ dependence of the effective interaction $W(\mathbf{q})$. In particular, relaxing the approximation Eq. (A3) and starting with a three-dimensional Fourier transform of Eq. (A1) yields an effective interaction

of the form

$$W(\mathbf{q}) = \int \frac{dq_z}{2\pi} V(\mathbf{q},q_z) n_{\rm el}^{\rm atom}(-\mathbf{q},-q_z) n_{\rm ion}^{\rm atom}(\mathbf{q},q_z). \quad \text{(A12)}$$

Further insight into the deformation potential might be gleaned by expanding this approach to include the three-dimensional Coulomb potential, following the approach introduced by Woods and Mahan who used the total density to avoid the $q \to 0$ divergence. For the present analysis, we simply view $D_{\rm DP}$ as a parameter to be fitted, and the $\mathbf{q}$ dependence $D_{\rm DP}(\mathbf{q})$ to be given by Eq. (A8) as a reasonable representative functional dependence.

APPENDIX B: PHONON MODEL

In this appendix, we list for completeness the details of the phonon model that we use throughout this paper. It is based on a model given in Appendix A of Ref. [64], but we are using a different coordinate system, so here we will specify the dynamical matrix as used in our calculations.

The in-plane phonon frequencies $\omega_{\mathbf{q}}^{\mu}$ and their polarization vectors $\vec{\eta}_j^{\mu}(\mathbf{q})$ ($j = 1,2$ for the two atoms in the basis) are obtained from a numerical solution of the phonon eigenvalue equation, neglecting out-of-plane phonon modes (see, for example, Ref. [84]). As illustrated in Fig. 1, we use a notation and geometry, adapted from Ref. [17], in which the two basis atoms are chosen to lie on a horizontal axis, and atom 1 (2) is the right (left) atom, with two-dimensional displacement vector $\vec{\eta}_1^{\mu}$ ($\vec{\eta}_2^{\mu}$). For this geometry, the phonon eigenvalue equation equivalent to that derived in Ref. [64] reads

$$(\hbar\omega^{\mu})^2 \begin{bmatrix} \eta_{1x}^{\mu} \\ \eta_{1y}^{\mu} \\ \eta_{2x}^{\mu} \\ \eta_{2y}^{\mu} \end{bmatrix} = (\widehat{D}_{\rm bs} + \widehat{D}_{\rm bb}) \begin{bmatrix} \eta_{1x}^{\mu} \\ \eta_{1y}^{\mu} \\ \eta_{2x}^{\mu} \\ \eta_{2y}^{\mu} \end{bmatrix}, \quad \text{(B1)}$$

where the bond stretching dynamical matrix is

$$\widehat{D}_{\rm bs} = \bar{K}_1 \begin{pmatrix} \frac{3}{2} & 0 & h_3 & -h_2 \\ 0 & \frac{3}{2} & -h_2 & h_1 \\ h_3^* & -h_2^* & \frac{3}{2} & 0 \\ -h_2^* & h_1^* & 0 & \frac{3}{2} \end{pmatrix}, \quad \text{(B2)}$$

and the bond-bending dynamical matrix reads

$$\widehat{D}_{\rm bb} = \bar{K}_2 \begin{pmatrix} h_6 & -h_5 & 6h_1 & 6h_2 \\ -h_5^* & h_4 & 6h_2 & 6h_3 \\ 6h_1^* & 6h_2^* & h_6 & -h_5^* \\ 6h_2^* & 6h_3^* & -h_5 & h_4 \end{pmatrix}, \quad \text{(B3)}$$

with the matrix elements

$$h_1(\mathbf{q}) = -\frac{3}{2} e^{iq_x a_L/(2\sqrt{3})} \cos\left(\frac{q_y a_L}{2}\right), \quad \text{(B4)}$$

$$h_2(\mathbf{q}) = i\frac{\sqrt{3}}{2} e^{iq_x a_L/(2\sqrt{3})} \sin\left(\frac{q_y a_L}{2}\right), \quad \text{(B5)}$$

$$h_3(\mathbf{q}) = -e^{-iq_x a_L/\sqrt{3}} - \frac{1}{2} e^{iq_x a_L/(2\sqrt{3})} \cos\left(\frac{q_y a_L}{2}\right), \quad \text{(B6)}$$

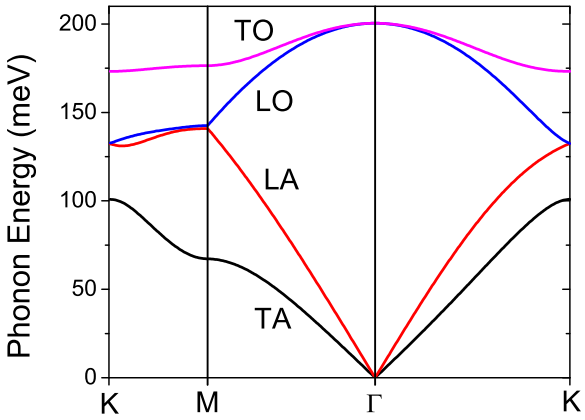

FIG. 15. The phonon dispersion diagram for the in-plane branches.

$$h_4(\mathbf{q}) = 7 + \sin^2\left(\frac{q_y a_L}{2}\right) + 2\cos\left(\frac{q_y a_L}{2}\right)\cos\left(\frac{\sqrt{3}}{2} q_x a_L\right), \quad \text{(B7)}$$

$$h_5(\mathbf{q}) = \sqrt{3} i e^{i\sqrt{3}q_x a_L/2} \sin\left(\frac{q_y a_L}{2}\right) - i\frac{\sqrt{3}}{2}\sin(q_y a_L), \quad \text{(B8)}$$

$$h_6(\mathbf{q}) = 9 - 3\sin^2\left(\frac{q_y a_L}{2}\right). \quad \text{(B9)}$$

The normalization of the phonon modes is $|\eta_{1x}^{\mu}|^2 + |\eta_{1y}^{\mu}|^2 + |\eta_{2x}^{\mu}|^2 + |\eta_{2y}^{\mu}|^2 = 1$, and we choose the y component of $\vec{\eta}_{\mu 1}$ to be purely real for all $\mathbf{q}$. We use the parameter values $\bar{K}_1 = 0.01$ (eV)^2, and $\bar{K}_2 = 0.0565\bar{K}_1$ [64]. Figure 15 shows the phonon dispersion obtained from this model, and Fig. 16 shows the eigenvectors across the entire Brillouin zone. Note that, according to Eq. (14), the eigenvector for atom 2 is not periodic in reciprocal space.

We note that in the small $\mathbf{q}$ limit, the acoustic branches are, to linear order in $\mathbf{q}$ [64],

$$\hbar\omega_{\mathbf{q}}^{\rm TA} = q a_L \sqrt{\frac{3}{2}\frac{\bar{K}_1\bar{K}_2}{\bar{K}_1 + 6\bar{K}_2}}, \quad \text{(B10)}$$

$$\hbar\omega_{\mathbf{q}}^{\rm LA} = q a_L \sqrt{\frac{3}{2}\frac{\bar{K}_1\bar{K}_2}{\bar{K}_1 + 6\bar{K}_2} + \frac{1}{8}\bar{K}_1}, \quad \text{(B11)}$$

where a_L is the lattice constant. Furthermore, the two-dimensional eigenvectors of atom 1 and 2 become identical in this limit,

$$\vec{\eta}_1^{\rm TA} = \vec{\eta}_2^{\rm TA} = \frac{1}{\sqrt{2}q}\begin{pmatrix} -q_y \\ q_x \end{pmatrix}, \quad \text{(B12)}$$

$$\vec{\eta}_1^{\rm LA} = \vec{\eta}_2^{\rm LA} = \frac{1}{\sqrt{2}q}\begin{pmatrix} q_x \\ q_y \end{pmatrix}. \quad \text{(B13)}$$

It is clear from Fig. 16 that at away from the zone center the two eigenvectors of atom 1 and 2 are not identical anymore. Furthermore, away from the zone center they are not real-valued, purely transverse, or purely longitudinal anymore.

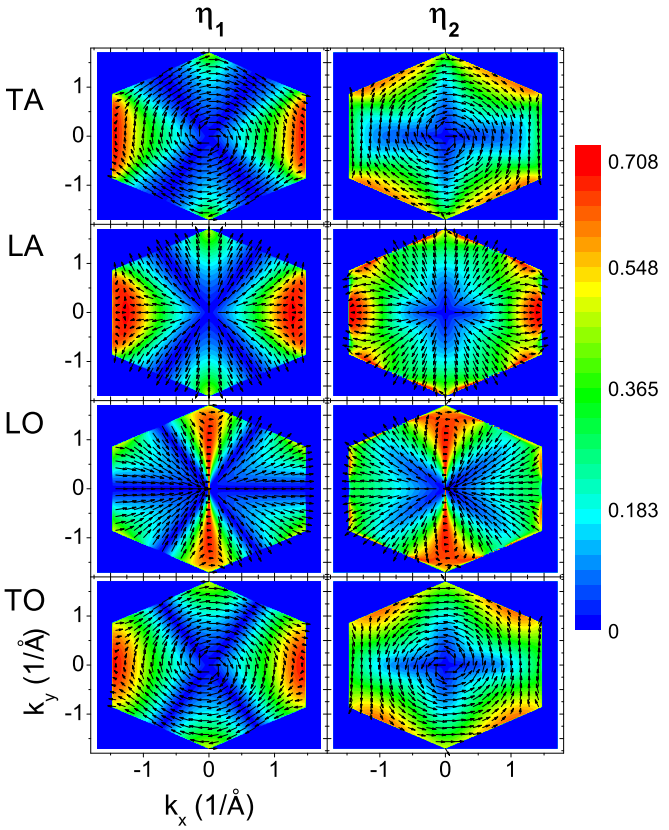

FIG. 16. The vector contour plots of the complex-valued two-dimensional displacement vectors η_1 and η_2 corresponding to the phonon branches in Fig. 15. The real part of the vectors are shown as arrows, and the magnitude of the imaginary part as color contour.

APPENDIX C: ABSENCE OF DIVERGENCES IN HIGHER BRILLOUIN ZONES

A potential singularity problem in the deformation potential contribution to the self-energy [Eqs. (27) and (28)] may arise at $\mathbf{k}-\mathbf{k}'=\mathbf{G}_u$, where $\mathbf{G}_u$ is any reciprocal lattice vector, due to the vanishing of $\omega^{LA,TA}_{\mathbf{k}-\mathbf{k}'}$ at these points. We consider a possible compensating zeroing of $W^{\rm DP}_{\rm LA}$ and $W^{\rm DP}_{\rm TA}$ here, see Eq. (21). We consider first the case $\mathbf{G}_u=\mathbf{0}$ and then the case $\mathbf{G}_u\neq\mathbf{0}$.

1. $\mathbf{k}-\mathbf{k}'=\mathbf{q}\in BZ$

We consider the point $\mathbf{q}=\mathbf{0}$ and hence $\mathbf{k}=\mathbf{k}'$. By this we imply in the following the limit of $\mathbf{q}\to\mathbf{0}$ where the phonon vectors $\vec{\eta}_{\mu i}(\mathbf{q})$ are well-defined for any small but nonzero $\mathbf{q}$. To show the vanishing of $\omega^{LA,TA}_{\mathbf{q}=\mathbf{0}}$, it can be seen from Eq. (21) that one needs to show

$$\sum_{\mathbf{G}} W(-\mathbf{G})\mathbf{G}[1+e^{i\mathbf{G}\cdot\vec{\delta}_1}][1+ss'e^{-i\mathbf{G}\cdot\vec{\delta}_1}]=\mathbf{0}, \qquad \text{(C1)}$$

where we have used $\vec{\eta}_{\mu 1}(\mathbf{q})=\vec{\eta}_{\mu 2}(\mathbf{q})$, which is valid in the small $\mathbf{q}$ limit and omitted the common factor of $\vec{\eta}_{\mu 1}(\mathbf{q})$. Equation (C1) would not be generally true for an arbitrary function $W(\mathbf{G})$. Some assumptions on W's behavior need to be taken.

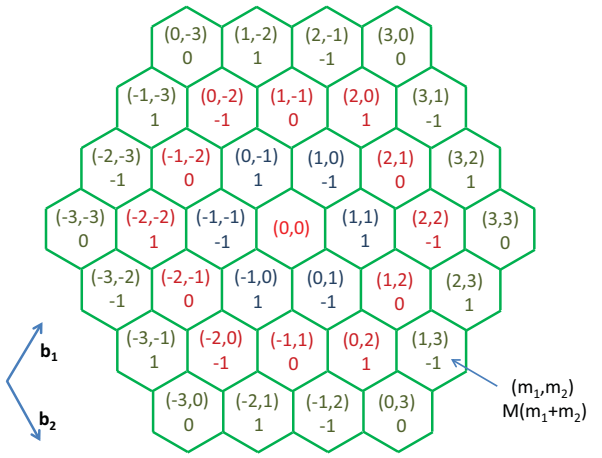

FIG. 17. Sketch of the first Brillouin zone, labeled (0,0), and three rings surrounding the first BZ.

a. *Intra(electron)band scattering: $s=s'$*

Equation (C1) can be proven in this case with the weak assumption $W(-\mathbf{G})=W(\mathbf{G})$. Under this assumption, the factor $W(-\mathbf{G})[1+e^{i\mathbf{G}\cdot\vec{\delta}_1}][1+e^{-i\mathbf{G}\cdot\vec{\delta}_1}]$ is invariant under the substitution $\mathbf{G}\to-\mathbf{G}$, while the factor $\mathbf{G}$ acquires a minus sign. So, the summand in Eq. (C1) is odd under $\mathbf{G}\to-\mathbf{G}$, and the sum is zero.

b. *Inter(electron)band scattering: $s=-s'$*

This case appears to be more difficult, and instead of a general proof, we restrict ourselves to the assumption that $W(\mathbf{G})$ is the same for all $\mathbf{G}$'s in the same ring of reciprocal space cells around the first Brillouin zone, and proceed as follows. We outline a general strategy for the proof, and we check that Eq. (C1) is indeed valid for the $\mathbf{G}$ sum over each ring up to the third ring, see Fig. 17.

The rings are numbered by $j=1,2,3,\ldots$ outwards from the first ring around the first BZ. We consider the sum over the jth ring and denote the common value of W in this ring by $W(\mathbf{G}\in j\text{th ring})=W_j$. The left-hand side of Eq. (C1) reduces to

$$\sum_{\mathbf{G}\in j\text{th ring}} W(-\mathbf{G})\mathbf{G}[1+e^{i\mathbf{G}\cdot\vec{\delta}_1}][1-e^{-i\mathbf{G}\cdot\vec{\delta}_1}]$$
$$=2iW_j\sum_{\mathbf{G}\in j\text{th ring}}\mathbf{G}\sin(\mathbf{G}\cdot\vec{\delta}_1). \qquad \text{(C2)}$$

The summand is even under $\mathbf{G}\to-\mathbf{G}$ and so the argument in the intraband case does not apply here. $\mathbf{G}$ can be written as $\mathbf{G}=m_1\mathbf{b}_1+m_2\mathbf{b}_2$, where $\mathbf{b}_1=\frac{2\pi}{3a}(\hat{x}+\sqrt{3}\hat{y})$, $\mathbf{b}_2=\frac{2\pi}{3a}(\hat{x}-\sqrt{3}\hat{y})$ are the basis vectors in reciprocal space, and m_1, m_2 are integers. This gives

$$\sin(\mathbf{G}\cdot\vec{\delta}_1)=-\sin[(m_1+m_2)2\pi/3]=\frac{\sqrt{3}}{2}M(m_1+m_2), \qquad \text{(C3)}$$

where

$$M(m_1+m_2) = 0 \quad \text{for } m_1+m_2 \text{ being a multiple of 3,}$$
$$= 2\mathrm{mod}(m_1+m_2,3)-3 \quad \text{otherwise.}$$

For example, for $m_1+m_2=-4,-3,\ldots,3,4$, the corresponding values for $M(m_1+m_2)$ are, respectively, $1,0,-1,1,0,-1,1,0,-1$. Equation (C2) is then given by

$$\frac{2\pi}{\sqrt{3}a} W_j i \sum_{\substack{m_1,m_2 \\ (j\text{th ring})}} [(m_1+m_2)\hat{x}+\sqrt{3}(m_1-m_2)\hat{y}]M(m_1+m_2), \tag{C4}$$

where the sum goes over values of m_1,m_2 that give $\mathbf{G}$'s lying in the jth ring. We note that if one $\mathbf{G}$ is given by $k\mathbf{b}_1+n\mathbf{b}_2$, then its mirror image across the x axis is given by $n\mathbf{b}_1+k\mathbf{b}_2$, which implies that the contributions to the y component of Eq. (C4) from a $\mathbf{G}$ and its mirror image cancel each other. The $\mathbf{G}$'s in a ring are paired up as mirror images across the x axis except for those lying on the x axis, each of which is of the form $n(\mathbf{b}_1+\mathbf{b}_2)$ and yields zero to the y component of Eq. (C4). Therefore Eq. (C4) reduces to $\frac{2\pi}{\sqrt{3}a} W_j i\hat{x} \sum_{\substack{m_1,m_2 \\ (j\text{th ring})}} (m_1+m_2)M(m_1+m_2)$, and one needs to show

$$\sum_{\substack{m_1,m_2 \\ (j\text{th ring})}} (m_1+m_2)M(m_1+m_2) = 0. \tag{C5}$$

The coordinates (m_1,m_2) and the functional values of $M(m_1+m_2)$ are shown in Fig. 17 for the innermost three rings. It is easy to see that Eq. (C5) is satisfied for each of these rings.

2. $\mathbf{k}-\mathbf{k}'-\mathbf{G}_u=\mathbf{Q}\in BZ$ and $\mathbf{G}_u\neq 0$

We reduce this case to the case discussed above. For this, we set $\mathbf{q}=\mathbf{0}$ and hence $\mathbf{k}=\mathbf{k}'+\mathbf{G}_u$. Then the factor in $W^{\mathrm{DP}}_{LA,TA}$ becomes

$$\sum_{\mathbf{G}} W(\mathbf{G}_u-\mathbf{G})(\mathbf{G}-\mathbf{G}_u) \times [1+e^{i(\mathbf{G}-\mathbf{G}_u)\cdot\vec{\delta}_1}][1+ss'e^{-i(\mathbf{G}-\mathbf{G}_u)\cdot\vec{\delta}_1}], \tag{C6}$$

where we have used $\phi(\mathbf{k}'+\mathbf{G}_u)=\phi(\mathbf{k}')+\mathbf{G}_u\cdot\vec{\delta}_1$. We substitute the dummy variable $\mathbf{G}\to\mathbf{G}'\equiv\mathbf{G}-\mathbf{G}_u$ and see that the summed part of Eq. (C6) is the same as the left-hand side of Eq. (C1), which was shown to vanish to the extent explained above.

[1] K. S. Novoselov, V. I. Fal'ko, L. Colombo, P. R. Gellert, M. G. Schwab, and K. Kim, Nature (London) **490**, 192 (2012).
[2] F. Bonaccorso, Z. Sun, T. Hasan, and A. C. Ferrari, Nat. Photon. **4**, 611 (2010).
[3] P. Avouris, Nano Lett. **10**, 4285 (2010).
[4] Emre O. Polat and Coskun Kocabas, Nano Lett. **13**, 5851 (2013).
[5] S. H. Mousavi, I. Kholmanov, K. B. Alici, D. Purtseladze, N. Arju, K. Tatar, D. Y. Fozdar, J. W. Suk, Y. F. Hao, A. B. Khanikaev, R. S. Ruoff, and G. Shvets, Nano Lett. **13**, 1111 (2013).
[6] I. T. Kim, A. Magasinski, K. Jacob, G. Yushin, and R. Tannenbaum, Carbon **52**, 56 (2013).
[7] S. H. Lee, J. Choi, H. D. Kim, H. Choi, and B. Min, Sci. Rep. **3**, 2135 (2013).
[8] A. Saynatjoki, L. Karvonen, J. Riikonen, W. Kim, S. Mehravar, R. A. Norwood, N. Peyghambarian, H. Lipsanen, and K. Kieu, ACS Nano **7**, 8441 (2013).
[9] J. H. Warner, F. Schäffel, A. Bachmatiuk, and M. H. Rümmeli, *Graphene - Fundamentals and Emergent Applications* (Elsevier, Waltham, 2013).
[10] I. Baylam, M. N. Cizmeciyan, S. Ozharar, E. O. Polat, C. Kocabas, and A. Sennaroglu, Opt. Lett. **39**, 5180 (2014).
[11] W. S. Koh, C. H. Gan, W. K. Phua, Y. A. Akimov, and P. Bai, IEEE J. Sel. Top. Quantum Electron. **20**, 4000107 (2014).
[12] T. Chu and Z. H. Chen, ACS Nano **8**, 3584 (2014).
[13] A. Y. Nikitin, P. Alonso-Gonzalez, and R. Hillenbrand, Nano Lett. **14**, 2896 (2014).
[14] *Physics of Graphene*, edited by H. Aoki and M. S. Dresselhaus (Springer-Verlag, Berlin, 2014).
[15] Nima Dabidian, Iskandar Kholmanov, Alexander B. Khanikaev, Kaya Tatar, Simeon Trendafilov, S. Hossein Mousavi, Carl Magnuson, Rodney S. Ruoff, and Gennady Shvets, ACS Photon. **2**, 216 (2015).
[16] A. Bostwick, T. Ohta, T. Seyller, K. Horn, and E. Rotenberg, Nat. Phys. **3**, 36 (2007).
[17] A. H. Castro-Neto, F. Guinea, N. M. R. Peres, K. S. Novoselov, and A. K. Geim, Rev. Mod. Phys. **81**, 109 (2009).
[18] Andreas Knorr, *Graphene and Carbon Nanotubes: Ultrafast Optics and Relaxation Dynamics*, 1st ed. (Wiley-VCH, Heidelberg, 2013).
[19] A. C. Ferrari, Solid State Commun. **143**, 47 (2007).
[20] D. Graf, F. Molitor, K. Ensslin, C. Stampfer, A. Jungen, C. Hierold, and L. Wirtz, Nano Lett. **7**, 238 (2007).
[21] L. M. Malard, J. Nilsson, D. C. Elias, J. C. Brant, F. Plentz, E. S. Alves, A. H. Castro Neto, and M. A. Pimenta, Phys. Rev. B **76**, 201401(R) (2007).
[22] L. M. Malard, M. A. Pimenta, and G. Dreselhaus, Phys. Rep. **473**, 51 (2009).
[23] Julio C. Chacon-Torres, Ludger Wirtz, and Thomas Pichler, ACS Nano **7**, 9249 (2013).
[24] J. M. Dawlaty, S. Shivaraman, M. Chandrashekhar, F. Rana, and M. G. Spencer, Appl. Phys. Lett. **92**, 042116 (2008).
[25] D. Sun, Z. K. Wu, C. Divin, X. B. Li, C. Berger, W. A. de Heer, P. N. First, and T. B. Norris, Phys. Rev. Lett. **101**, 157402 (2008).
[26] R. W. Newson, J. Dean, B. Schmidt, and H. M. van Driel, Opt. Express **17**, 2326 (2009).
[27] Yuanbo Zhang, Tsung-Ta Tang, Caglar Girit, Zhao Hao, Michael C. Martin, Alex Zettl, Michael F. Crommie, Y. Ron Shen, and Feng Wang, Nature (London) **459**, 820 (2009).
[28] B. A. Ruzicka, S. Wang, L. K. Werake, B. Weintrub, K. P. Loh, and H. Zhao, Phys. Rev. B **82**, 195414 (2010).

[29] M. Breusing, S. Kuehn, T. Winzer, E. Malic, F. Milde, N. Severin, J. P. Rabe, C. Ropers, A. Knorr, and T. Elsaesser, Phys. Rev. B **83**, 153410 (2011).

[30] D. Sun, C. Divin, C. Berger, W. A. de Heer, P. N. First, and T. B. Norris, Phys. Status Solidi C **8**, 1194 (2011).

[31] B. Y. Sun, Y. Zhou, and M. W. Wu, Phys. Rev. B **85**, 125413 (2012).

[32] K. M. Dani, J. Lee, R. Sharma, A. D. Mohite, C. M. Galande, P. M. Ajayan, A. M. Dattelbaum, H. Htoon, A. J. Taylor, and R. P. Prasankumar, Phys. Rev. B **86**, 125403 (2012).

[33] T. Stroucken, J. H. Gronqvist, and S. W. Koch, J. Opt. Soc. Am. B **29**, A86 (2012).

[34] D. Sun, C. Divin, M. Mihnev, T. Winzer, E. Malic, A. Knorr, J. E. Sipe, C. Berger, W. A. de Heer, P. N. First, and T. B. Norris, New J. Phys. **14**, 105012 (2012).

[35] B. Y. Sun and M. W. Wu, Phys. Rev. B **88**, 235422 (2013).

[36] B. Y. Sun and M. W. Wu, New J. Phys. **15**, 083038 (2013).

[37] L. M. Malard, K. F. Mal, A. H. Castro Neto, N. M. R. Peres, and T. F. Heinz, New J. Phys. **15**, 015009 (2013).

[38] J. L. Cheng, N. Vermeulen, and J. E. Sipe, New J. Phys. **16**, 053014 (2014).

[39] I. Al-Naib, J. E. Sipe, and M. M. Dignam, Phys. Rev. B **90**, 245423 (2014).

[40] K. F. Mak, F. H. da Jornada, K. L. He, J. Deslippe, N. Petrone, J. Hone, J. Shan, S. G. Louie, and T. F. Heinz, Phys. Rev. Lett. **112**, 207401 (2014).

[41] P. Bowlan, E. Martinez-Moreno, K. Reimann, T. Elsaesser, and M. Woerner, Phys. Rev. B **89**, 041408 (2014).

[42] A. Majumdar, J. Kim, J. Vuckovic, and F. Wang, IEEE J. Sel. Top. Quantum Electron. **20**, 4600204 (2014).

[43] V. N. Kotov, B. Uchoa, V. M. Pereira, F. Guinea, and A. H. Castro-Neto, Rev. Mod. Phys. **84**, 1067 (2012).

[44] E. G. Mishchenko, Phys. Rev. Lett. **98**, 216801 (2007).

[45] R. A. Jishi, L. Venkataraman, M. S. Dresselhaus, and G. Dresselhaus, Chem. Phys. Lett. **209**, 77 (1993).

[46] M. Scheuch, T. Kampfrath, M. Wolf, K. von Volkmann, and C. Frischkorn, Appl. Phys. Lett. **99**, 211908 (2011).

[47] P. T. Araugo, D. L. Mafra, K. Saito, R. Saito, J. Kong, and M. S. Dresselhaus, Phys. Rev. Lett. **109**, 046801 (2012).

[48] G. D. Sanders, A. R. T. Nugraha, K. Sato, J. H. Kim, J. Kono, R. Saito, and C. J. Stanton, J. Phys.: Condens. Matter **25**, 144201 (2013).

[49] B. V. Cunning, K. Ishioka, C. L. Brown, and D. Kielpinski, Appl. Phys. Lett. **104**, 181907 (2014).

[50] Cheol-Hwan Park, Feliciano Giustino, Marvin L. Cohen, and Steven G. Louie, Phys. Rev. Lett. **99**, 086804 (2007).

[51] M. Calandra and F. Mauri, Phys. Rev. B **76**, 205411 (2007).

[52] C. H. Park, F. Giustino, M. L. Cohen, and S. G. Louie, Nano Lett. **8**, 4229 (2008).

[53] K. Kaasbjerg, K. S. Thygesen, and K. W. Jacobsen, Phys. Rev. B **85**, 165440 (2012).

[54] D. A. Siegel, C. Y. Hwang, A. V. Fedorov, and A. Lanzara, New J. Phys. **14**, 095006 (2012).

[55] C. H. Park, N. Bonini, T. Sohier, G. Samsonidze, B. Kozinsky, M. Calandra, F. Mauri, and N. Marzari, Nano Lett. **14**, 1113 (2014).

[56] T. Sohier, M. Calandra, C. H. Park, N. Bonini, N. Marzari, and F. Mauri, Phys. Rev. B **90**, 125414 (2014).

[57] D. H. Chae, T. Utikal, S. Weisenburger, H. Giessen, K. von Klitzing, M. Lippitz, and J. Smet, Nano Lett. **11**, 1379 (2011).

[58] K. F. Mak, J. Shan, and T. F. Heinz, Phys. Rev. Lett. **106**, 046401 (2011).

[59] L. Yang, J. Deslippe, C. H. Park, M. L. Cohen, and S. G. Louie, Phys. Rev. Lett. **103**, 186802 (2009).

[60] K. Oum, T. Lenzer, M. Scholz, D. Y. Jung, O. Sul, B. J. Cho, J. Lange, and A. Muller, J. Phys. Chem. C **118**, 6454 (2014).

[61] A. T. Roberts, R. Binder, N. H. Kwong, D. Golla, D. Cormode, B. J. LeRoy, H. O. Everitt, and A. Sandhu, Phys. Rev. Lett. **112**, 187401 (2014).

[62] F. Kadi, T. Winzer, E. Malic, A. Knorr, F. Göttfert, M. Mittendorff, S. Winnerl, and M. Helm, Phys. Rev. Lett. **113**, 035502 (2014).

[63] L. M. Woods and G. D. Mahan, Phys. Rev. B **61**, 10651 (2000).

[64] H. Suzuura and T. Ando, Phys. Rev. B **65**, 235412 (2002).

[65] G. G. Samsonidze, E. B. Barros, R. Saito, J. Jiang, G. Dresselhaus, and M. Dresselhaus, Phys. Rev. B **75**, 155420 (2007).

[66] H. Suzuura and T. Ando, J. Phys. Soc. Jpn. **77**, 044703 (2008).

[67] G. D. Mahan and L. M. Woods, Phys. Rev. B **60**, 5276 (1999).

[68] W. K. Tse and S. Das Sarma, Phys. Rev. Lett. **99**, 236802 (2007).

[69] F. Rana, J. H. Strait, H. N. Wang, and C. Manolatou, Phys. Rev. B **84**, 045437 (2011).

[70] E. H. Hwang and S. Das Sarma, Phys. Rev. B **77**, 115449 (2008).

[71] T. Low, V. Perebeinos, R. Kim, M. Freitag, and P. Avouris, Phys. Rev. B **86**, 045413 (2012).

[72] V. Perebeinos and P. Avouris, Phys. Rev. B **81**, 195442 (2010).

[73] H. K. Min, E. H. Hwang, and S. Das Sarma, Phys. Rev. B **83**, 161404 (2011).

[74] J. Schiefele, F. Sols, and F. Guinea, Phys. Rev. B **85**, 195420 (2012).

[75] J. Gonzalez and E. Perfetto, New J. Phys. **11**, 095015 (2009).

[76] Tsuneya Ando, J. Phys. Soc. Jpn. **75**, 124701 (2006).

[77] N. Mounet and N. Marzari, Phys. Rev. B **71**, 205214 (2005).

[78] N. Bonini, M. Lazzeri, N. Marzari, and F. Mauri, Phys. Rev. Lett. **99**, 176802 (2007).

[79] K. M. Borysenko, J. T. Mullen, E. A. Barry, S. Paul, Y. G. Semenov, J. M. Zavada, M. B. Nardelli, and K. W. Kim, Phys. Rev. B **81**, 121412 (2010).

[80] S. Ulstrup, M. Bianchi, R. Hatch, D. D. Guan, A. Baraldi, D. Alfe, L. Hornekaer, and P. Hofmann, Phys. Rev. B **86**, 161402 (2012).

[81] C. Thomsen, S. Reich, and P. Ordejon, Phys. Rev. B **65**, 073403 (2002).

[82] N. Sule and I. Knezevic, J. Appl. Phys. **112**, 053702 (2012).

[83] O. Madelung, *Introduction of Solid-State Theory*, 1st ed. (Springer-Verlag, Heidelberg, 1978).

[84] L. Pietronero, S. Strössler, H. Zeller, and M. J. Rice, Phys. Rev. B **22**, 904 (1980).

[85] J. L. Manes, Phys. Rev. B **76**, 045430 (2007).

[86] E. Mariani and F. von Oppen, Phys. Rev. Lett. **100**, 076801 (2008).

[87] E. Mariani and F. von Oppen, Phys. Rev. B **82**, 195403 (2010).

[88] L. W. Nordheim, Ann. Phys. **9**, 607 (1931).

[89] G. D. Whitfield, Phys. Rev. **121**, 720 (1961).

[90] V. M. Pereira, A. H. Castro Neto, and N. M. R. Peres, Phys. Rev. B **80**, 045401 (2009).

[91] N. W. Ashcroft and N. D. Mermin, *Solid State Physics* (Holt, Rinehart and Winston, Dumfries, NC, 1976).
[92] R. Saito, G. Dresselhaus, and M. Dresselhaus, *Physical Properties of Carbon Nanotubes*, 1st ed. (World Scientific Publishing Co., London, 1998).
[93] Z. Li and J. P. Carbotte, Phys. Rev. B **88**, 045417 (2013).
[94] Z. Li and J. P. Carbotte, Eur. Phys. J. B **88**, 87 (2015).
[95] G. D. Mahan, *Many-Particle Physics* (Plenum Press, New York, 1986).
[96] Z. Li, C. J. Chandler, and F. Marsiglio, Phys. Rev. B **83**, 045104 (2011).
[97] Li Yang, Phys. Rev. B **83**, 085405 (2011).
[98] Z. Li and J. P. Carbotte, Phys. Rev. B **88**, 195133 (2013).
[99] E. Clementi and C. Roetti, At. Data Nucl. Data Tables **14**, 177 (1974).
[100] C. Hwang, D. A. Siegel, S. K. Mo, W. Regan, A. Ismach, Y. G. Zhang, A. Zettl, and A. Lanzara, Sci. Rep. **2**, 590 (2012).